Responses to Reviewer 1

This is a WRF-Chem modeling study using a case of summertime convection in Houston from the ACPC Model Intercomparison Project. The focus is on the indirect aerosol effects on deep convection, using both SBM and Morrison microphysical schemes. The paper is certainly within the scope of ACP. It is well organized and clearly written, with adequate introduction and scientific review. The goals of the study, as elucidated in the first paragraph of section 5, are to (1) evaluate the performance of the WRF-Chem-SBM scheme, (2) explore the differences in aerosol effects on deep convective clouds produced by the SBM and Morrison schemes, and (3) explore the major factors responsible for the differences. The first two goals are descriptive in nature, they are fulfilled and clearly documented. However, I found the deductions made regarding the third goal to be questionable and poorly-supported by the data presented. The manuscript concludes that, the "warm-phase invigoration" effect is absent with the Morrison scheme, and this is "mainly due to limitations of the saturation adjustment approach for droplet condensation and evaporation calculation". While the saturation adjustment is probably the root cause, I find it unlikely that it is the DIRECT cause of the simulated sensitivities. Other processes have to be involved, and they need to be identified and properly analyzed. I'll elaborate on this in my specific comments. This flaw needs to be addressed before the manuscript is published.

We thank the reviewer for recognizing the importance of our study and the nice summary. The reviewer's comment about through what interactions the saturation adjustment does not lead to the convective invigoration as the explicit supersaturation approach is very constructive. We have done more analysis with three figures added (Fig. 16-18). Our detailed response is provided as below.

Specific Comments:

There are three sets of model sensitivity tests using either realistic anthropogenic aerosol loadings or no anthropogenic aerosol: the explicit SBM scheme, the 2-moment Morrison scheme with saturation adjustment technic, and the Morrison scheme improved with a super saturation formula. The SBM scheme simulated stronger convection and more aerosol sensitivity compared with the original Morrison scheme, whereas the improved Morrison scheme produced results and sensitivities closer to the SBM results. The conclusion followed was that ". . .the saturation adjustment method for the condensation and evaporation calculation is mainly responsible for the limited aerosol effects with the Morrison scheme." This should be the correct conclusion, that the limitations in saturation adjustment are the root cause of the simulated differences in sensitivities. However, it cannot be the DIRECT cause. I can think of two pieces of evidence to support my assertion.

1. In the conclusion, the authors stated: ". . .the saturation adjustment method actually leads to a smaller condensation latent heating than the explicit calculation with supersaturation. . ." (L407). Fig. 12b was given to support the statement. However, saturation adjustment cannot be the direct reason for the smaller latent heating in Fig. 12b (or in any of the plots in Figs. 11~14). Figs. 11~14 only showed mean vertical profiles of various variables for the "top 25 percentiles" of the simulated updrafts. The main reason the Morrison scheme has smaller latent heating in Fig. 12b is not because of the saturation adjustment, it is because the updrafts are weaker (Fig. 11 a, b).

The dynamics already determined the differences in the latent heating, buoyancy, condensation rate, et al. shown in Figs. 11~14, not the other way around. In other words, the top 25 percentile of the updrafts are already weaker in the Morrison scheme simulation. As a result, latent heating should be weaker. Whether saturation adjustment causes this or not cannot be established by Figs. 11~ 14.

2. If saturation adjustment were the immediate/main cause of the simulated sensitivities, then the original Morrison scheme should produce stronger convection than SBM, given the same aerosol loading. This is because the saturation adjustment converts ALL supersaturation into cloud water, and thus should release the most latent heating among all schemes used. The fact that the SBM_anth case has much stronger convection than MOR_anth clearly precludes this possibility. If the authors plot Fig. 12 for the same vertical velocity (or super saturation), the Morrison scheme should have more latent heating, not less. In conclusion, the saturation adjustment cannot be the direct cause of the simulated sensitivities. Something else must interact with it to cause these sensitivities. The authors actually observed the oddity of their conclusion in their conclusion, L401~L405. They noted that their study differs from Lebo et al. (2012). In this sense, Lebo et al. (2012) gave a feasible explanation, that the the "cold-phase invigoration" is in play together with saturation adjustment. The current case study may or may not have the same mechanism. Nevertheless, the authors need to find the missing link between the saturation adjustment, which produces the maximum possible latent heating by eliminating all super saturation, and the enhanced convection when super saturation is allowed.

Thanks for the constructive comments. We addressed (1) and (2) together here since both of them are for the same issue: why the saturation adjustment approach leads to smaller condensational heating than the explicit supersaturation approach in Morrison Scheme and through what interactions it did not lead to the convective invigoration as the explicit supersaturation approach did.

As added in Line 416-444, "Now we explain why the saturation adjustment approach leads to smaller condensational heating than the explicit supersaturation approach in Morrison Scheme and why it leads to a smaller sensitivity to aerosols compared with the explicit supersaturation approach. We examine the time evolution of latent heating, updraft, and hydrometeor properties. At the warm cloud stage at 1700 UTC, the saturation adjustment indeed produces more condensational latent heating which leads to larger buoyancy and stronger updraft intensity compared to the explicit supersaturation because of removing supersaturation (Fig. 16, left, blue vs. orange). By the time of 1900 UTC when the clouds have developed into mixed-phase clouds, the saturation adjustment produces less condensational heating and weaker convection than the explicit supersaturation approach (Fig. 16, middle). The results remain similarly later at the deep cloud stage 2100 UTC (Fig. 16, right).

How does this change happen from 1700 to 1900 UTC? At the warm cloud stage (17:00 UTC), the saturation adjustment produces droplets with larger sizes (up to 100% larger for the mean radius) than the explicit supersaturation because of more cloud water produced as a result of zeroing-out supersaturation at each time step (droplet formation is similar between the two cases as shown in Fig. 13). This results in much faster and larger warm rain, while with the explicit supersaturation rain number and mass are absent at 1700 UTC as shown in Fig. 17d and 18d). As a result, when evolving into the mixed-phase stage (19:00 UTC), much fewer cloud droplets are transported to the levels above the freezing level (Fig. 17b and 18b). Whereas with the explicit supersaturation, because of the delayed/suppressed warm rain and smaller droplets (the mean

radius is decreased from 8 to 6 μm at 3 km), much more cloud droplets are lifted to the higher levels. Correspondingly, a few times higher total ice particle number and mass are seen compared with the saturation adjustment (Fig. 17g and 18g) because more droplets above the freezing level induce stronger ice processes (droplet freezing, riming, and deposition). This leads to more latent heat release (Fig. 16e), which increases the buoyancy and convective intensity. With the explicit supersaturation, increasing aerosols leads to a larger reduction in droplet size (up to 1 μm more in the mean radius) than the saturation adjustment, therefore more enhanced ice microphysical processes and the larger latent heat. Besides, the condensational heating is more enhanced by aerosols with the explicit supersaturation (Fig. 16). Together, a much larger sensitivity to aerosols is seen with the explicit supersaturation."

Another result that puzzles me comes from Fig. 9a, where the high aerosol loading cases (SBM_anth and MOR_anth) rain earlier than the low aerosol cases. Why? The conventional wisdom is the opposite. High aerosol loading will produce more, smaller cloud droplets, reducing auto conversion and delaying surface rainfall onset. Can this be checked and explained?

The warm rain is very weak (analysis box averaged rain rate at ~0.02 mm hr-1) and the time period is short (~10min), so the delay of warm rain is too hard to be shown from Fig. 9a. We do see the delay of warm rain by aerosols but only about 5 min (probably due to the humid condition of the case study). We have added the following clarifications to the revised manuscript in Line 335-339, "Note Fig. 9a shows that anthropogenic aerosols lead to an earlier start of the precipitation with both SBM and Morrison, which reflects the faster transition of warm rain to mixed-phase precipitation. We do see the delay of warm rain by aerosols but only about 5 min (probably due to the humid condition of the case study), which is difficult to be shown in Fig. 9a since averaged rain rate for the analysis box is ~0.02 mm hr-1 and the time period is very short (~10 min)".

Responses to Reviewer 2

This manuscript presents results of numerical simulations that consider impacts of cloud microphysics parameterization on convective clouds near Houston. Overall, this is an impressive study that includes simulation and validation of aerosols that play key role in cloud dynamics and microphysics, and subsequently investigates the CCN impact on convective dynamics. My main problem is with the context of this study and with the interpretation of model results. Obviously, the authors are strongly for the invigoration and I am one of those who oppose their views as scientifically unjustified. The manuscript should provide less biased view of the invigoration and needs to include additional analysis of model results as suggested in my specific comments.

We thank the reviewer for your time and constructive comments. Our detailed point-by-point responses are provided below. As the reviewer is one of those who oppose the convective invigoration concept, we are standing at the other side as one of those who support the concept based on our theoretical analysis and modeling studies (but we do not mean that it occurs in every case since in reality many other factors are in play). The two sides of arguments have been existing for a while, and it is not the role of this paper to resolve this issue. We have submitted a comment paper on Grabowski and Morrison (2020, 2016) to J. Atmos. Sci. to detail the theoretical analysis and modeling designs between the two arguments, which would allow both sides to further discuss there.

Major comments:

1. The introduction needs to provide a better context for this work. A brief discussion of invigoration in the second paragraph of the introduction is misleading. It presents the authors view that is not supported by simple arguments and by other studies. For instance, the "cold-phase invigoration" as described in lines 42-45 is simply not possible because the latent heat released by freezing the cloud water carried across the melting level in the polluted case only balances the weight of the water carried upwards. So where does the invigoration come from? The explanation of the "warm-phase invigoration" is simply incorrect and it repeats the incorrect argument used in papers the authors cite. The latent heating does not depend on the droplet concentration and droplet radius as long as the updraft velocity does not change. This is strictly true when the in-cloud supersaturation is equal to the quasi-equilibrium supersaturation. The validity of the quasi-equilibrium supersaturation approximation has been argued in many studies, at least in the absence of ice (e.g., Politovich and Cooper JAS 1988). Such an incorrect interpretation is repeated in lines 334-337. I suggest the authors consult the recently accepted manuscript by Grabowski that provides a thorough discussion of the two invigorations, see section 2 there. The manuscript is available on EOR in JAS (https://journals.ametsoc.org/doi/abs/10.1175/JAS-D-20-0012.1). I also suggest the authors consult and cite a paper by Varble (JAS 2018) for a less biased discussion of the invigoration problem.

We put our responses to the convective invigoration questions that the reviewer raised separately at the end of this file to avoid a distraction. Here, in the introduction, we have added text to provide different arguments existing in literature.

For the cold-phase invigoration, we have added in Line 51-56 "Grabowski and Morrison (2016; 2020) rejected this invigoration concept by arguing that the increase in the buoyancy by freezing

is completely offset by the buoyancy for carrying the extra cloud water across the freezing level. However, Rosenfeld et al. (2008) showed that the buoyancy restores and increases after the precipitation of the ice hydrometeors that form upon freezing of the high supercooled liquid water content into large graupel and hail (Rosenfeld et al., 2008)".
For the warm-phase invigoration, we have added in Line 63-71 "Grabowski and Morrison (2020) proposed a different interpretation of the warm-phase invigoration from the literature listed above. They argued that condensation rates only depend on updraft velocity with the quasi-steady assumption (i.e., the true supersaturation is approximated with the equilibrium supersaturation), therefore they interpreted that it is the lower equilibrium supersaturation in polluted conditions that lead to a larger buoyancy, thus enhanced updraft speeds, and condensation. Several studies showed that the quasi-steady assumption is invalidated in the conditions of low droplet concentrations (Politovich and Cooper, 1988; Korolev and Mazin, 2003) or acceleration of vertical velocity (Pinsky et al., 2013)".
We also added text of "Meteorological buffering effects were also found for aerosol effects on convective clouds over a large region and sufficiently long-time (over a few days and weeks) simulations (Stevens and Feingold, 2009; van den Heever et al., 2011). Dagan et al. (2019) showed that the lifetimes of cloud systems are mostly much shorter than that and rarely reach this buffering state" in Line 75-79 and "Confidently isolating and quantifying an aerosol deep convective invigoration effect from observations requires very long-term measurements: data of 10 years are still not enough over the South Great Plains due to the large variability of meteorological conditions (Varble, 2018)" in Line 80-83.

2. The discussion of bulk versus bin microphysics starting in l. 61 misses an important point: not all bulk schemes apply saturation adjustment. For instance, the scheme of Morrison and Grabowski (JAS 2007, 2008a,b) allows supersaturation to evolve. The scheme shows a good agreement with bin microphysics in simple tests. This is important for the context of simulations described in the manuscript under review.

What we said is that saturation adjustment is an often-used approach in bulk scheme, so our description should have no problem. But we have added a sentence to describe the bulk schemes used the explicit supersaturation, i.e., "Some bulk schemes take the explicit supersaturation approach to allow supersaturation to evolve (e.g., Li et al., 2008; 2009a; Morrison and Grabowski 2007, 2008)." (Line 92-93).

3. The setup of model simulations is not clear to me. I understand the motivation for applying the same boundary conditions for the inner domain in all simulations and hence using the MERRA-2 data on the inner-domain boundaries. However, how this is done with the outer domain present in not clear to me. Is it fair to say that outer domain is ran initially without the inner domain to simulate aerosol evolution and then the inner domain simulations are run without the outer domain using boundary conditions from MERRA-2 for the dynamics and thermodynamics, and applying the outer domain data for the aerosols? In other words, simulations with the two nested domains are actually never run together, correct? If my understanding is correct, then the description on p. 8 and 9 needs to change along my suggestion above. Also, it would be useful to describe in more detail the vertical grid structure. The 51 levels suggest quite a low vertical resolution.

Yes, two nested domains were run separately, and the purpose of running outer domain is to get a good estimation of aerosol fields to feed to inner domain for the initial and boundary chemical and aerosol conditions. We have added a sentence in Line 179-181 to clearly state this, "The simulations for Domain 1 and Domain 2 are run separately and the Domain 1 simulations serve to provide the chemical and aerosol lateral boundary and initial conditions of Domain 2."
The 51 vertical grid levels allow 50-100m resolution below 2-km altitude and ~500 m above it (added in Line 178-179), which is not very high resolution but not too bad.

4. The description of the simulation setup mentions 3-member ensembles. However, the ensemble information is never shown in the discussion of results. I think this is important because one may wonder to what extent a specific realization of the convection development affects the comparison. In other words, are the differences systematic or coincidental? All profiles shown in the figures should include the ensemble spread. Also, Fig. 7 should show all ensemble members and not just one realization. Specifically, is the more organized bin microphysics convection present in all ensemble members when compared to a more scattered bulk convection, or is this true only for the example shown in Fig. 7?

We presented the ensemble mean results in most of the analysis results for Domain 2 simulations. As the reviewer suggested, in the revised manuscript, we added the shaded areas for the ensemble spread for all the profile figures (Fig. 9a and Fig.11-14). For the spatial distribution figure (Fig. 7), we now show the results for each ensemble member. Yes, SBM has more organized convection than MOR in all three ensemble members. This information has been added to Line 297-298, "All three ensemble members consistently show smaller but more scattered convective cells with the Morrison scheme compared with SBM".

5. Although never mentioned in the manuscript, the vertical resolution near the cloud base is too low to properly resolve CCN activation in the bin scheme. It is well known that the vertical grid length around 10 m is needed to resolve the cloud base supersaturation maximum. Poor representation of cloud base activation affects droplet concentrations. In fact, droplet concentrations simulated by the two schemes are never compared in the paper. This key parameter should be analyzed and presented. Should the bin scheme use parameterization of the cloud base CCN activation as the Morrison scheme?

The droplet nucleation rate (i.e., aerosol activation rate) was indeed shown in Figure 13. The droplet nucleation rates simulated by SBM is comparable with the parameterization used in Morrison scheme, as shown in Figure 13. In this response letter, we also further showed the spatial distribution of droplet number concentration at cloud base: droplet number concentration at cloud bases in SBM_anth are similar with the observation and MOR_anth in magnitudes, suggesting the SBM is doing an okay job in cloud base activation.

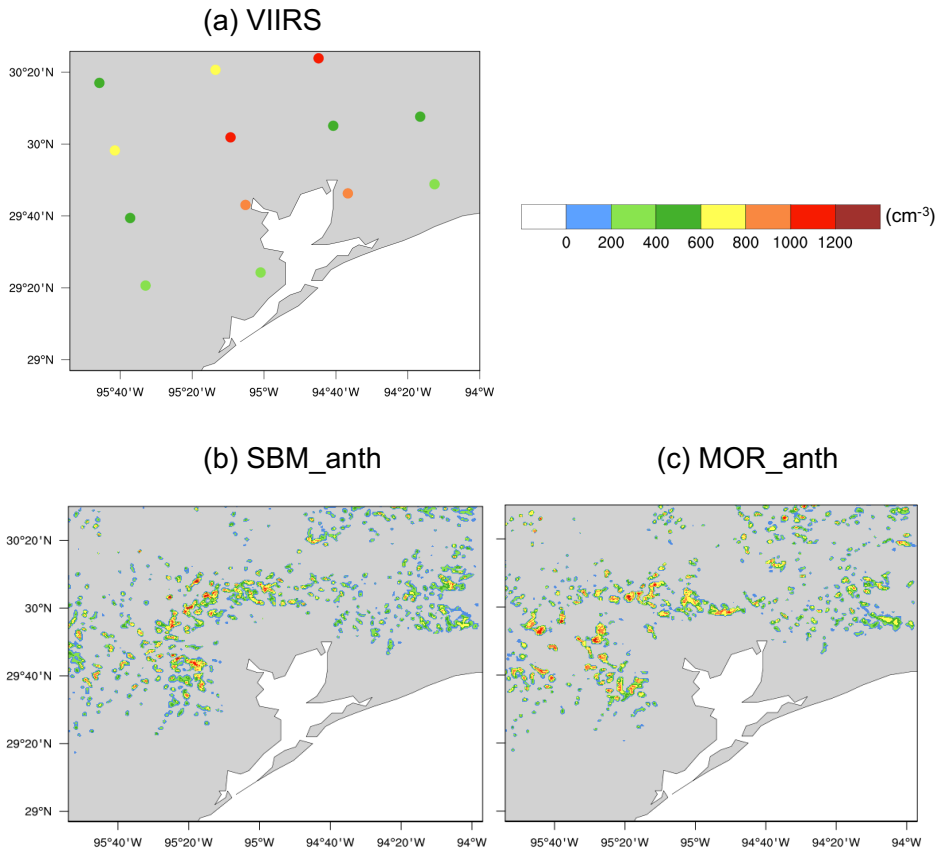

Fig. r1 CCN number concentration at cloud base from (a) VIIRS satellite retrieved at 1943 UTC (Rosenfeld et al. 2016) and model simulation (b) SBM_anth, (c) MOR_anth at 2000 UTC, 19 June 2013.

6. Saturation adjustment and its role in the simulations. I think this aspect is poorly represented in the manuscript. First, one needs to clearly explain that saturation adjustment affects cloud buoyancy and thus simulated vertical velocity. The impact on the cloud buoyancy has been shown theoretically in Grabowski and Jarecka (JAS 2015) and discussed in the context of deep convection simulation in Grabowski and Morrison (JAS 2017). There are two aspects: 1) the increase of the vertical velocity because of the increased buoyancy (that does lead to the increased condensation), and 2) the increase of the condensation rate when the updraft is the same (this is because reducing supersaturation to zero gives more condensation). One way to separate the two effects is to show the condensation rate for a given vertical velocity (at a given height) and then repeat it for different vertical velocities. And do it separately for bin and bulk schemes. I expect that in undiluted or weakly diluted cloudy volumes the condensation rate is similar for the same vertical velocity in the two schemes and for the two aerosol conditions. I leave it to the authors to figure out what it means if my prediction turns out correct. Note that such an analysis eliminates the impact of different convection realizations and properly demonstrates the impact of the microphysics scheme on the condensation rate.

For the role of saturation adjustment, we have added more analysis as shown in Fig. 16-18 and two paragraphs (Line 416-444) to the revised manuscript, also to address a comment from Reviewer #1.

"Now we explain why the saturation adjustment approach leads to smaller condensational heating than the explicit supersaturation approach in Morrison Scheme and why it leads to a smaller sensitivity to aerosols compared with the explicit supersaturation approach. We examine the time evolution of latent heating, updraft, and hydrometeor properties. At the warm cloud stage at 1700 UTC, the saturation adjustment indeed produces more condensational latent heating which leads to larger buoyancy and stronger updraft intensity compared to the explicit supersaturation because of removing supersaturation (Fig. 16, left, blue vs. orange). By the time of 1900 UTC when the clouds have developed into mixed-phase clouds, the saturation adjustment produces less condensational heating and weaker convection than the explicit supersaturation approach (Fig. 16, middle). The results remain similarly later at the deep cloud stage 2100 UTC (Fig. 16, right).

How does this change happen from 1700 to 1900 UTC? At the warm cloud stage (17:00 UTC), the saturation adjustment produces droplets with larger sizes (up to 100% larger for the mean radius) than the explicit supersaturation because of more cloud water produced as a result of zeroing-out supersaturation at each time step (droplet formation is similar between the two cases as shown in Fig. 13). This results in much faster and larger warm rain, while with the explicit supersaturation rain number and mass are absent at 1700 UTC as shown in Fig. 17d and 18d). As a result, when evolving into the mixed-phase stage (19:00 UTC), much fewer cloud droplets are transported to the levels above the freezing level (Fig. 17b and 18b). Whereas with the explicit supersaturation, because of the delayed/suppressed warm rain and smaller droplets (the mean radius is decreased from 8 to 6 μm at 3 km), much more cloud droplets are lifted to the higher levels. Correspondingly, a few times higher total ice particle number and mass are seen compared with the saturation adjustment (Fig. 17g and 18g) because more droplets above the freezing level induce stronger ice processes (droplet freezing, riming, and deposition). This leads to more latent heat release (Fig. 16e), which increases the buoyancy and convective intensity. With the explicit supersaturation, increasing aerosols leads to a larger reduction in droplet size (up to 1 μm more in the mean radius) than the saturation adjustment, therefore more enhanced ice microphysical processes and the larger latent heat. Besides, the condensational heating is more enhanced by aerosols with the explicit supersaturation (Fig. 16). Together, a much larger sensitivity to aerosols is seen with the explicit supersaturation".

To satisfy the reviewer's curiosity about the relationship of condensation rate and vertical velocity, we plot their relationships in the simulations with the two schemes and for the two aerosol conditions at two different heights over the period 16-18 UTC where the warm cloud dominated (Fig. r2 and r3). For the same updraft velocity, the Morrison scheme with the saturation adjustment predicted larger condensation rates compared with SBM as expected because reducing supersaturation to zero gives more condensation (Fig. r2-r3, left vs right). The larger condensation rate leads to larger buoyancy and therefore strong updraft velocity as shown in Fig. 17. With the anthropogenic aerosols added, the condensation rate is not changed much with the saturation adjustment at both altitudes (right panels in Fig. r2-r3) because the approach removes the dependence of condensation on droplet properties. However, in the bin scheme, we find that SBM_anth tends to have larger condensation rates for the same updrafts than SBM_noanth (Fig. r3, a vs c) above cloud base where the increase of cloud droplet number is significant (Fig. 15a). This clearly shows that higher droplet number has larger condensation rate for the same vertical velocity, which is different from what the reviewer predicted because the reviewer's argument is that that the condensation rate is only dependent on updraft, not droplet

properties, which is true for saturation adjustment approach, not for the explicit calculation in SBM.

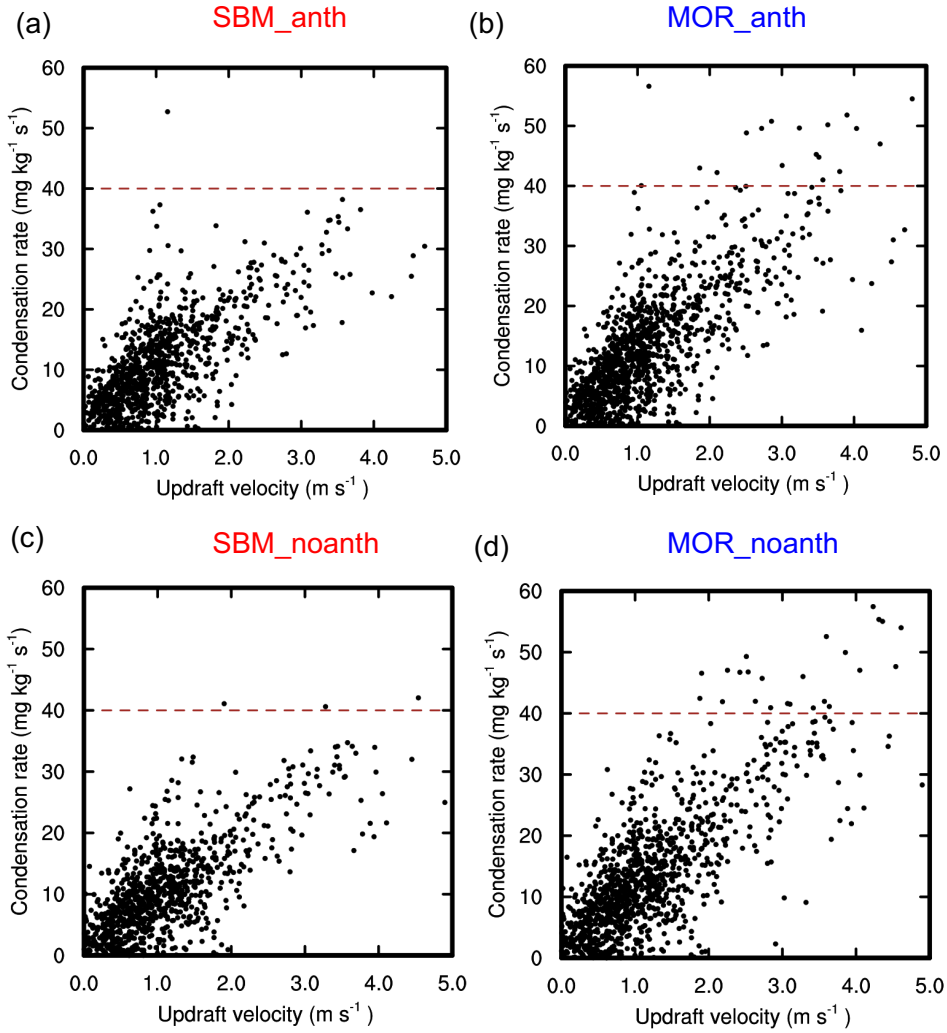

Figure r2 The relationship between condensation rate and updraft velocity at 1.7 km (near cloud base) for SBM_anth, SBM_noanth, MOR_anth and MOR_noanth at warm cloud stage (1600 – 1800 UTC).

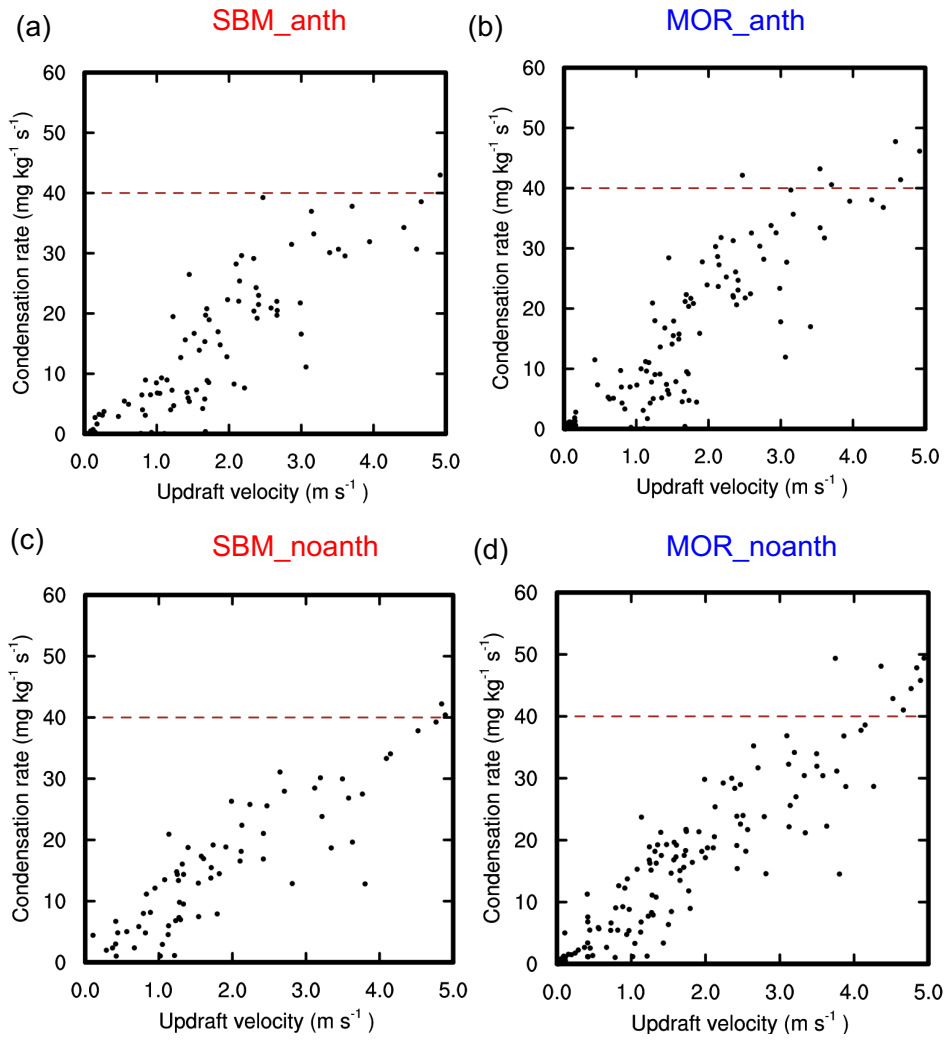

Figure r3 Same as Figure r2, but for 3 km altitude.

7. Saturation adjustment may also affect the way ice processes are simulated. Grabowski and Morrison (JAS 2017) document some possible impacts. This aspect begs the question about the representation of ice processes in the two schemes. I expect there are differences that are never discussed in the paper. Specifically, are ice concentrations similar between the two schemes? If there are significant differences, these have significant implications for the simulated cloud processes. As with the cloud droplet concentrations, this is never shown and discussed in the paper.

See our response to comment #6. The saturation adjustment weakens the ice processes due to less droplets remaining for being lifted above freezing level as a result of efficient conversion from cloud droplet to rain because of larger condensational growth. We also add the findings of Grabowski and Morrison (JAS 2017) in the discussion session: "Grabowski and Morrison (2017) also showed that the saturation adjustment affected ice processes by producing larger ice particles with larger falling velocities compared with the explicit supersaturation approach, leading to the reduction of anvil clouds." (Line 477-479).

We have added a figure for the hydrometeor number concentrations (Figure 15) corresponding to the mass mixing ratios shown in Figure 14.

8. Related to some of the points above: How different is the supersaturation simulated by the bin scheme from the quasi-equilibrium supersaturation below the freezing level? The quasi-equilibrium supersaturation can be derived from the local updraft velocity and droplet spectral characteristics. I expect the two are quite close in undiluted or weakly diluted cloudy volumes as suggested by other studies. If so, then please see comment 1 above.

The quasi-equilibrium supersaturation is much larger than simulated supersaturation between 3-5 km with more than 10 s relaxation time, which is mainly due to low droplet number. Please see Fig. r5 for more details.

Specific comments:
1. The abstract requires revisions after major comments above are addressed.

A new key point has been added to the abstract. That is "Whereas such an effect is absent with the Morrison two-moment bulk microphysics, mainly because the saturation adjustment approach for droplet condensation and evaporation calculation removes the dependence of condensation on droplet properties and limits the ice processes by a more efficient conversion of droplets into raindrops, which leads to less cloud droplets being transported to the altitudes above the freezing level" (Line 25-29).

2. Grabowski and Jarecka (2015) show that the key impact in shallow convection simulations is the way saturation adjustment affects cloud edge evaporation (either resolved or because of the numerical diffusion). This aspect is never mentioned in the manuscript under review, but perhaps the cloud water evaporation plays some role, for instance, by driving stronger cloud-edge downdrafts when saturation adjustment is used.

We added a sentence to the discussion part: "The increased condensation is significant for the enhanced warm clouds when saturation adjustment is used. This is different from the points of Grabowski and Jarecka (2015) that the cloud edge evaporation effect is more important for the nonprecipitating shallow clouds" (Line 479-482).

3. L. 162: The grid length of the MERRA data should be mentioned here.

The MERRA data is at the resolution of 0.5° × 0.625°. This information was indeed included, and now it is at Line 183-184, "meteorological lateral boundary and initial conditions were created from MERRA-2 at the resolution of 0.5° × 0.625°(Gelaro et al., 2017)."

4. L 198: Rather than sending the reader to Lebo et al. (2012), please explain what is meant by "explicit representation of supersaturation over a time step". Is this close to the quasi-equilibrium supersaturation?

We have added a sentence to describe it after that sentence since we do not think it is needed to copy the equation from Lebo et al. 2012 and put there, i.e., "That is the supersaturation is solved

by the source and sink terms of dynamic forcing and condensation/evaporation within an one-timestep" (Line 226-228).

5. L. 229. I would not call the agreement shown in Fig. 3 "very good". This would imply that a color inside each circle is as in the background. This is not the case in several circles. Similar comment applies to Figs. 4 – 6. I understand the difficult task the model faces, but being honest about the simulation drawbacks would be appropriate. For instance, in Fig. 6, the temperature and wind simulations are closer to each other than to the observations.

We have added text to point out the simulation drawbacks. At Line 258-260, "Though not exactly the same, the values from D1_MOR_anth show a similar distribution with the observations in terms of the surface PM2.5 averaged over 24 hours (the day before the convection near Houston)." Also at Line 281-285: "Compared with the coarse resolution NLDAS data, both SBM_anth and MOR_anth capture the general temperature pattern with a little overestimation at the northeast part of the domain (mainly rural area) . The modeled southerly winds do not reach further north as the NLDAS data, possibly because of the feedback of the small-scale features which are simulated with the high resolution to mesoscale circulations."

6. What is "thermal buoyancy"? I think this is just "buoyancy", correct? Please change.

Thermal buoyancy is the buoyancy contributed from temperature and moisture perturbation. We have added a note about this. Buoyancy can be attributed to temperature and moisture perturbation and condensate loading. The net buoyancy is the sum of thermal buoyancy and condensate loading.

7. Fig. 8. To me, the simulations look close to each other and different than the NEXRAD picture. Is the plot for all three ensemble members? This needs to be clearly stated.

Yes, this is for all three ensemble members. This information is now added to the figure captions. The major differences between the two simulations are at the low (<12 dBZ) and high large reflectivity (> 48 dBZ).

8. Fig. 9. Again, are the plots for all ensemble members? How large is the variability among the ensemble members? I suggest to show the total accumulation in addition to the rate. Total accumulation tends to eliminate the impact of statistical fluctuations due to different flow realizations.

Yes, this is for all three ensemble members. The shaded area shows the ensemble spread. We have also added the information of accumulated precipitation: "The observed accumulated rain over the time period shown in Fig. 9a is about 3.8 mm, both SBM_anth (~4.5 mm) and MOR_anth (~4.2 mm) overestimate the accumulated precipitation due to the longer rain period compared with the observations" (Line 313-316).

9. Fig. 10. Again, all ensemble members? How different are the figures for individual ensemble members? If they are much different, then more ensemble members are needed.

Yes, this is for all three ensemble members. The differences between the individual ensemble members is not very much. And also considering the expensive computation cost, we decide to keep at the current three members.

10. Fig. 13. Again, all ensemble members? What is the "drop nucleation rate"? Is this "CCN activation rate"? To what extent it is affected by the low vertical resolution?

Yes, this is for all three ensemble members. Droplet nucleation rate is also named as the CCN activation rate. The activate rates from SBM are shown ok. See our reply to the major comment #5

11. For figures 1 -14, it is not clear how the averaging is done. For instance, if there are differences in the number of updrafts but their strength does not change, some of those profiles would change as well, correct? I think one has to clearly explain how the averaging is done to get a clear picture of the processes involved. And document the ensemble spread. As an example, see section 6 in Grabowski's manuscript (JAS 2020, Early Online Release) that discusses the incorrect interpretation of the enhanced lighting over south-east Asia shipping lines. More latent heating may simply come from a larger number of convective updrafts, not necessarily stronger updrafts.

The average is done only over the grid points satisfying the thresholds described in each figure caption, meaning other grid points failed to meet the thresholds are not accounted for the average. We made this clear in the figure capture. The ensemble spread is marked as shaded areas for all profiles.
In our case the updraft speeds are indeed stronger, not because of more updrafts, as seen from the PDF figure (Figure 10).

Responses to the reviewer' questions about the cold-phase and warm-phase invigoration by aerosols.

The reviewer's comments:
It presents the authors view that is not supported by simple arguments and by other studies. For instance, the "cold-phase invigoration" as described in lines 42-45 is simply not possible because the latent heat released by freezing the cloud water carried across the melting level in the polluted case only balances the weight of the water carried upwards. So where does the invigoration come from? The explanation of the "warm-phase invigoration" is simply incorrect and it repeats the incorrect argument used in papers the authors cite. The latent heating does not depend on the droplet concentration and droplet radius as long as the updraft velocity does not change. This is strictly true when the in-cloud supersaturation is equal to the quasi-equilibrium supersaturation. The validity of the quasi-equilibrium supersaturation approximation has been argued in many studies, at least in the absence of ice (e.g., Politovich and Cooper JAS 1988). Such an incorrect interpretation is repeated in lines 334-337. I suggest the authors consult the recently accepted manuscript by Grabowski that provides a thorough discussion of the two invigorations, see section 2 there. The manuscript is available on EOR in JAS (https://journals.ametsoc.org/doi/abs/10.1175/JAS-D-20-0012.1). I also suggest the authors consult and cite a paper by Varble (JAS 2018) for a less biased discussion of the invigoration problem.

Here are the follow-on comments from the reviewer on the cold-phase and warm-phase invigoration.

I appreciate the authors' responses to my initial comments. However, the response has fundamental flaws and thus I cannot consider the issues settled. I think the authors need to reconsider my comments about the invigoration and correct obvious flaws in their arguments.

About the cold-phase invigoration:
The authors clearly misunderstood my argument. The figure below illustrates the starting point for my argument:

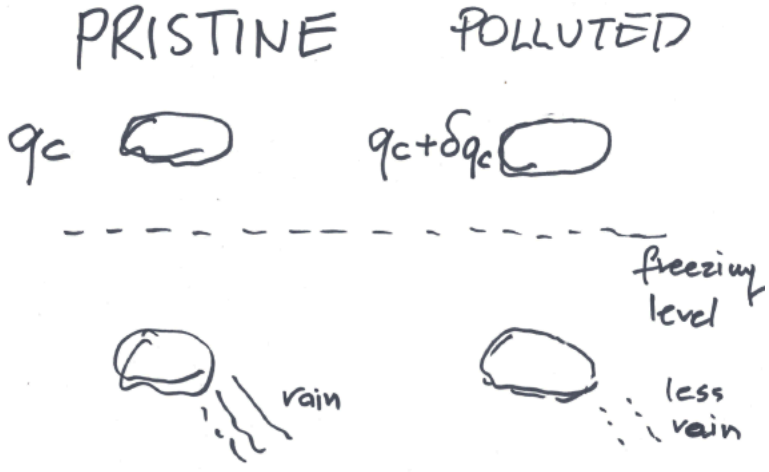

The left part of the panel shows a cloudy parcel that rises through the melting (freezing) level in pristine conditions. The total liquid condensate above the freezing level is q_c. The right part of

the figure shows situation when a similar parcel rises in polluted conditions. Because of the less efficient warm rain processes, the parcel above the freezing level carries more liquid condensate, $q_c + \delta q_c$. Freezing of δq_c in the authors' opinion (and in many other papers) is the reason for the invigoration. However, to carry δq_c across the freezing level requires extra buoyancy when compared to the left panel. As shown in section 2a of Grabowski and Morrison (2020), the two effects approximately balance each other. It follows the original sentences in the manuscript under review that say: "… a well-known theory is that increasing aerosol concentrations can suppress warm rain as a result of increased droplet number but reduced droplet size. This allows more cloud water to be lifted to a higher altitude wherein the freezing of this larger amount of cloud water induces larger latent heating associated with stronger ice microphysical processes, thereby invigorating convective updrafts…" are simply incorrect and require additional explanations. For instance, the invigoration would be possible if the frozen condensate was removed through precipitation processes.
That said, I really do not think referring to invigoration is needed for this manuscript. If the authors insist, then the introduction and references to the invigoration in the text should provide a less biased discussion, for instance, as in Grabowski and Morrison JAS papers and as in Varble (JAS 2018).

About the warm-phase invigoration:
The phase relaxation time scale and the quasi equilibrium supersaturation estimates in the authors' response above are simply wrong. Below I include a table from Politovich and Cooper (JAS 1988) that shows phase relaxation time scale for different combinations of droplet concentrations and radii. These values are much smaller than those shown in the authors' response.

TABLE 1. Time constant characterizing supersaturation.
(Values of $\tau = 1/(a_2 I)$ s for $p = 771$ mb, $T = 4.3°C$)

Radius (μm)	Droplet concentration (cm^{-3})			
	100	300	500	1000
2	14.1	4.7	2.8	1.4
3	8.7	2.9	1.7	0.87
5	4.9	1.6	0.98	0.49
10	2.3	0.77	0.46	0.23

The key question is why?
The explanation is relatively simple. The authors say that they use the formulas from Pinsky et al., eq. (4) therein. However, Pinsky et al. apply a simplified (and in my view incorrect) droplet growth equation that is different from the comprehensive formula used in Politovich and Cooper (JAS 1988). The key point is that one has to apply exactly the same droplet growth equation in the phase relaxation time scale calculation (and thus in the quasi-equilibrium supersaturation) as used in the numerical model. I expect Khain's bin microphysics applies a correct droplet growth formulation that is close to the one used in Politovich and Cooper (JAS 1988), and not the simplified droplet growth equation applied in Pinsky et al. The supersaturation simulated by the model can be compared to the diagnosed quasi-equilibrium supersaturation only if exactly the same droplet growth equations are used in both. This was the case for the relatively good agreement shown in Grabowski and Morrison (JAS 2017), at least below the freezing level, see Fig. 15 therein. In summary, the values shown in the authors' response above have to be

Corrected.
The above discussion requires the authors to modify their responses and revise their paper accordingly. Note that the second part of my rebuttal impacts some of my other original comments. I strongly object publication of the manuscript unless those comments are appropriately addressed

---

As we noted earlier, the two sides of arguments have been existing for a while, and it should not be the role of this paper to debate and resolve this issue. Here we only provided our key points, the detailed review and comment paper was submitted to J. Atmos. Sci., which would allow both sides to discuss and debate there. The bulk of the above comments are chiefly the expression of the reviewer's view on the aerosol invigoration effect, rather any substantial objection to the scientific importance and the findings of this study.

For the "cold-phase invigoration", the reviewer's argument "the increase in the buoyancy by freezing is completely offset by the buoyancy for carrying the extra cloud water across the freezing level" has several issues:
(1) Droplet ascending and then freezing are subsequent at different locations; also, the two processes can take at very different time scales (freezing is instant but ascending could take much longer time). How do they compensate each other at different time scale and locations? Responses of a complex non-linear dynamical system in deep convective clouds strongly depend on duration and location of the forcing.
(2) In the process of ascending in updrafts, droplets will grow through condensation, and the changes in latent heating and condensate loading from this are not considered in this argument.
(3) The argument neglected the subsequent enhanced riming and deposition resulting from more ice particles formed from enhanced droplet freezing. This leads to (a) a further increase in latent heating and (b) a reduction in condensate loading because more graupel and hail form due to increased supercooled liquid content and precipitate. Rosenfeld et al. (2008) indeed considered the possible compensation between the extra condensate loading and the extra latent heat of freezing. They showed (in line d of their Fig. 3) that the total buoyancy excesses and invigoration occurs after the ice hydrometeors are unloaded (i.e., precipitated) from the cloud parcel. The unloading is quite efficient in the case of rich supercooled liquid water content where large particles like graupel and hail can form. Many modeling studies have showed that the latent heat released from deposition and riming is much larger (at least an order of magnitude) than freezing. The increase in latent heating by aerosols is mainly from the increase in deposition and riming at the high-levels. Overall, the buoyancy increase via latent heat release exceeds the buoyancy decrease resulting from the increase in condensate loading, leading to a positive net buoyancy (e.g., Fan et al. 2012a, 2018; Tao and Li, 2016; Lebo et al. 2012; Chen et al. 2020).

For the "warm-phase invigoration", our interpretation of the mechanism is the enhanced condensation by larger droplet nucleation in the polluted conditions releases more latent heat, enhance buoyancy this updraft intensity. This is consistent with many literature studies (e.g., Khain et al. 2012; Igel et al. 2015; Sheffield et al. 2015; Chen et al. 2017; Fan et al. 2018; Lebo 2018). The reviewer argued that condensation rates only depend on updraft velocity with the quasi-steady assumption (i.e., true supersaturation is approximated with equilibrium supersaturation), therefore they interpreted that it is the lower equilibrium supersaturation in

polluted conditions that lead to a larger buoyancy, thus enhanced updraft speeds and condensation.

This quasi-steady assumption is neither physically justified for the strong updrafts of deep convective clouds nor is it suitable for studying aerosol effects on deep convective clouds which requires the exact solution of supersaturation. Previous studies (e.g., Politovich and Cooper 1988; Korolev and Mazin 2003, Pinsky et al. 2013) showed that the quasi-steady assumption is invalidated in conditions of (a) low droplet concentrations (pristine condition) and (b) intense condensation and evaporation (e.g., cloud base and strong updrafts) due to long relaxation time (larger than a few seconds). Note that both Politovich and Cooper (1988) and Korolev and Mazin (2003) evaluated the phase relaxation time under the assumption of the constant drop radius, which is not as accurate as Pinsky et al. (2013) that used the accurate equation for supersaturation. However, the reviewer mistakenly thought that Politovich and Cooper (1988) used an accurate droplet growth equation but Pinsky et al. (2013) used a simplified one.
So we followed Eq. 3 and Eq. 4 in Pinsky et al. (2013) to calculate Seq and phase relaxation time τ, respectively. Fig. r4 shows the calculated phase relaxation time as a function of droplet number and radius from SBM_anth. The values we got are quite consistent with the Table 1 of Politovich and Cooper (1988) for droplet number concentrations (Nc) of 100, 300, and 500 cm-3, which proves that our calculation has no problem. The reviewer said our values "are simply wrong" in his follow-on comment which were from the same calculation except we showed the mean value for the updrafts with a velocity greater than 2 m s−1 (Fig. r5). In these relatively strong updrafts, the phase relaxation time is long (Fig. r5c) because of low Nc (Fig. r5d) due to fast conversion of droplets to rain. Fig. r4 showed that most of the updrafts have Nc of 5-20 cm-3. The averaged τ for the updrafts greater than 2 m s−1 are around 10-15 s (with large values exceed 60 s). Above the cloud base, the quasi-equilibrium supersaturation is much higher than the true supersaturation (Fig. r5a) where low droplet number concentration (Fig. r5c) and strong updrafts (Fig. r5b) are seen. Therefore, it is clear that the short phase relaxation time (a few seconds) is only true near cloud base with large droplet number concentrations (~ hundreds cm-3) and weak updrafts. However, in relatively strong updrafts, the droplet number above the cloud base is much reduced (~ tens cm-3 in this case) due to fast conversion of droplets to rain, thus the phase relaxation time is much longer (> 10 s and even over 60 s) and the assumption of S=Seq is not valid any more. This is particularly true for the pristine case (SBM_noanth), we can see the Seq can be much higher than the true supersaturation (Fig. r2a), so assuming S=Seq would lead to a large bias in condensation and evaporation in the pristine case.

Therefore, appropriately simulating aerosol effects on deep convective clouds requires an exact supersaturation calculation (Eq. 6 in Pinsky et al. 2013), in which the condensation depends on droplet number and size, and more droplets in the polluted clouds increase condensation and decrease supersaturation, which clearly showed our interpretation is physically solid. In addition, as shown in our responses to the comment #6, we see the polluted case (SBM_anth) has larger condensation rates for the same updrafts than the pristine case (SBM_noanth) (Fig. r3, a vs c) above cloud base where the increase of cloud droplet number is significant (Fig. 15a). This clearly shows that higher droplet number leads to larger condensation rate for the same vertical velocity, which rebuts the reviewer' argument that condensate rates are similar under the same vertical velocity.

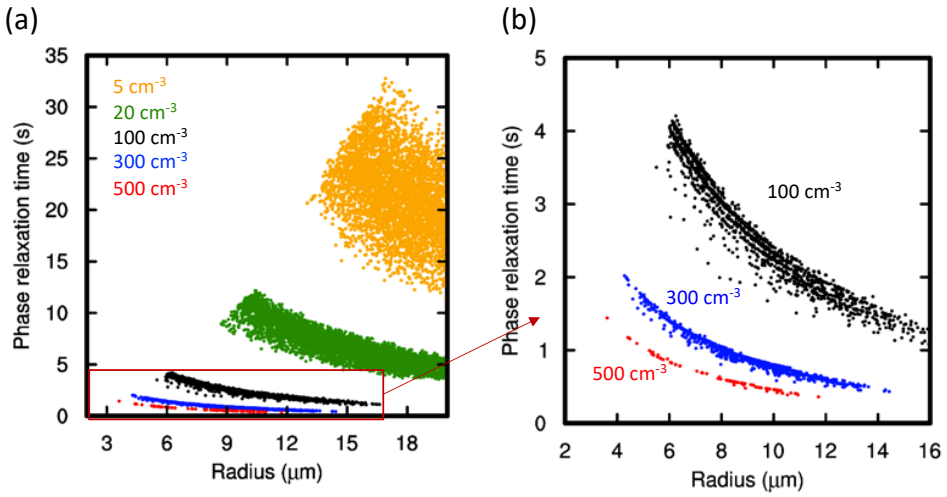

Figure r4 (a) Relationship between phase relaxation time and droplet radius for different droplet number concentrations from the simulations SBM_anth. (b) is the same as (a), except zooming in for droplet number concentrations of 100 cm^{-3}(black), 300 cm^{-3}(blue), 500 cm^{-3}(red).

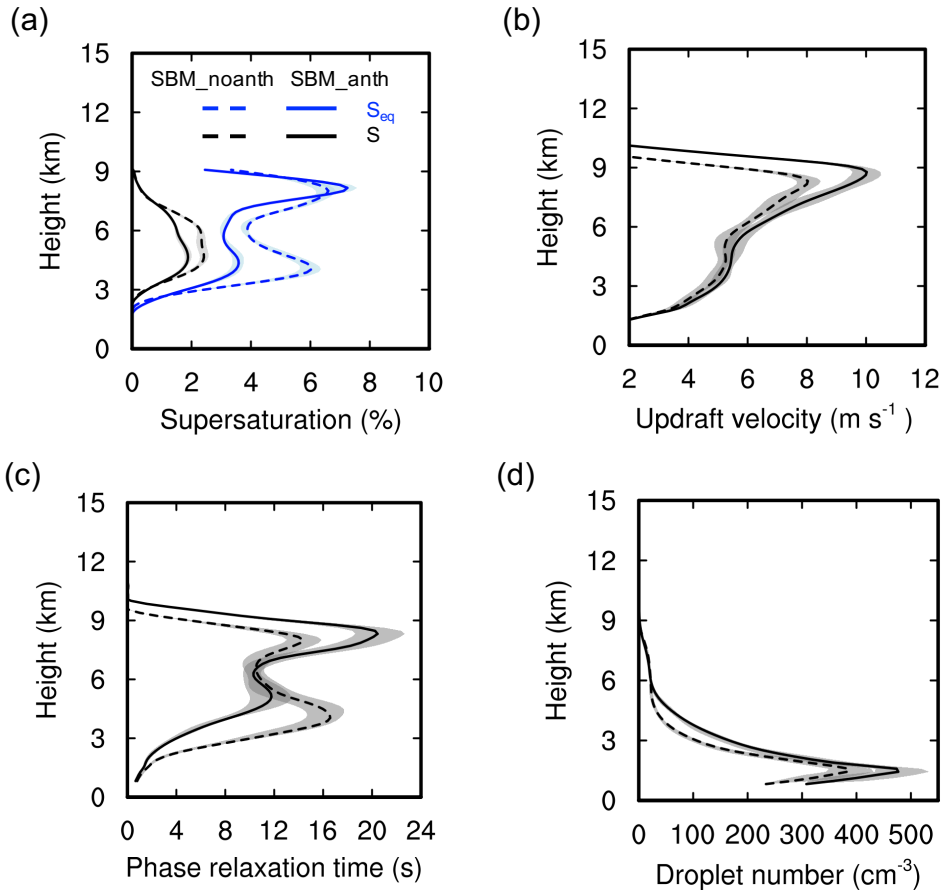

Figure r5 Vertical profiles of (a) supersaturation and quasi-equilibrium supersaturation, (b) updraft velocity, (c) phase relaxation time and (d) droplet number concentration averaged over the updrafts with value greater than 2 m s^{-1} from the simulations SBM_anth and SBM_noanth,

over the analysis domain as shown in the red box in Figure 7 during the strong convection period (2000 – 2300 UTC, 19 Jun 2013). The shaded areas mark the spread of ensemble runs.

Impacts of Cloud Microphysics Parameterizations on Simulated Aerosol-Cloud-Interactions for Deep Convective Clouds over Houston

Yuwei Zhang[1, 2], Jiwen Fan[2, *], Zhanqing Li[1], Daniel Rosenfeld[3]

[1]Department of Atmospheric and Oceanic Science, University of Maryland, College Park, MD, USA

[2]Atmospheric Sciences and Global Change Division, Pacific Northwest National Laboratory, Richland, WA, USA

[3] Institute of Earth Sciences, The Hebrew University of Jerusalem, Jerusalem, Israel

* *Correspondence to*: Jiwen Fan (jiwen.fan@pnnl.gov)

Abstract

Aerosol-cloud interactions remain largely uncertain in predicting their impacts on weather and climate. Cloud microphysics parameterization is one of the factors leading to the large uncertainty. Here we investigate the impacts of anthropogenic aerosols on the convective intensity and precipitation of a thunderstorm occurring on 19 June 2013 over Houston with the Chemistry version of Weather Research and Forecast model (WRF-Chem) using the Morrison two-moment bulk scheme and spectral-bin microphysics (SBM) scheme. We find that the SBM predicts a deep convective cloud agreeing better with observations in terms of reflectivity and precipitation compared with the Morrison bulk scheme that has been used in many weather and climate models. With the SBM scheme, we see a significant invigoration effect on convective intensity and precipitation by anthropogenic aerosols mainly through enhanced condensation latent heating (i.e., the warm-phase invigoration). Whereas such an effect is absent with the Morrison two-moment bulk microphysics, mainly because the saturation adjustment approach for droplet condensation and evaporation calculation removes the dependence of condensation on droplet properties and limits the ice processes by a more efficient conversion of droplets into raindrops, which leads to less cloud droplets being transported to the altitudes above the freezing level.

1 Introduction

Deep convective clouds (DCCs) produce copious precipitation and play important roles in the hydrological and energy cycle as well as regional and global circulation (e.g., Arakawa, 2004; Houze, 2014). DCCs and associated precipitation are determined by water vapor, vertical motion of air, and cloud microphysics that could be affected by aerosols through aerosol-radiative interactions (ARI) or aerosol-cloud interactions (ACI) or both. The cloud-mediated aerosol effects are recognized by the Intergovernmental Panel on Climate Change (IPCC) as one of the key sources of uncertainty in our knowledge of Earth's energy budget and anthropogenic climate forcing (e.g., Arakawa, 2004; Andreae et al., 2005; Haywood and Boucher, 2000; Lohmann and Feichter, 2005).

Precipitation, latent heat, and cloud radiative forcing associated with DCCs are strongly associated with cloud microphysical processes, which can be modulated by aerosols through serving as cloud condensation nuclei (CCN) and ice nuclei (IN). For aerosol-DCC interactions, a well-known theory is that increasing aerosol concentrations can suppress warm rain as a result of increased droplet number but reduced droplet size. This allows more cloud droplets to be lifted to altitudes above the freezing level, inducing stronger ice microphysical processes (e.g., droplet freezing, riming, and deposition) which release larger latent heating, thereby invigorating convective updrafts (referred to as "cold-phase invigoration,"; Khain et al. 2005; Rosenfeld et al., 2008). It is significant in the situations of warm-cloud bases (> 15°C; Fan et al., 2012b; Li et al., 2011; Rosenfeld et al., 2014; Tao and Li, 2016) and weak wind shear (Fan et al., 2009, 2012b, 2013; Li et al., 2008; Lebo et al., 2012). Grabowski and Morrison (2016; 2020) rejected this invigoration concept by arguing that the increase in the buoyancy by freezing is completely offset by the buoyancy for carrying the extra cloud water across the freezing level. However, Rosenfeld

et al. (2008) showed that the buoyancy restores and increases after the precipitation of the ice hydrometeors that form upon freezing of the high supercooled liquid water content into large graupel and hail.

Another theory is that increasing aerosols enhances droplet nucleation particularly secondary nucleation after warm rain initiates, which promotes condensation because of larger integrated droplet surface area associated with a higher number of small droplets (Fan et al., 2007, 2013, 2018; Koren at al., 2014; Lebo, 2018; Sheffield et al., 2015; Chen et al., 2020). This so-called "warm-phase invigoration", which is manifested in a warm, humid, and clean environment under which the addition of a large number of ultrafine aerosol particles from urban pollution leads to stronger invigoration than the "cold-phase invigoration" (Fan et al., 2018). Grabowski and Morrison (2020) proposed a different interpretation of the warm-phase invigoration from the literature listed above. They argued that condensation rates only depend on updraft velocity with the quasi-steady assumption (i.e., the true supersaturation is approximated with the equilibrium supersaturation), therefore they interpreted that it is the lower equilibrium supersaturation in polluted conditions that lead to a larger buoyancy, thus enhanced updraft speeds, and condensation. Several studies showed that the quasi-steady assumption is invalidated in the conditions of low droplet concentrations (Politovich and Cooper, 1988; Korolev and Mazin, 2003) or acceleration of vertical velocity (Pinsky et al., 2013).

Many factors can affect whether aerosols invigorate or suppress convective intensity through ACI, such as environmental wind shear (Fan et al., 2009; Lebo et al., 2012), relative humidity (Fan et al., 2007; Khain et al., 2008), and Convective Available Potential Energy (Lebo et al., 2012; Morrison, 2012; Storer et al., 2010). Meteorological buffering effects were also found for aerosol effects on convective clouds over a large region and long-time (over a few days and weeks)

77 simulations (Stevens and Feingold, 2009; van den Heever et al., 2011). Dagan et al. (2018) showed
78 that the lifetimes of cloud systems are mostly much shorter than that and rarely reach this buffering
79 state. For DCCs with complicated dynamics, thermodynamics, and microphysics, aerosol impacts
80 are extremely complex and still remain poorly known. Confidently isolating and quantifying an
81 aerosol deep convective invigoration effect from observations requires very long-term
82 measurements: data of 10 years are still not enough over the Southern Great Plains due to the large
83 variability of meteorological conditions (Varble, 2018).

84 Modeling of ACI is quite dependent on cloud microphysics parameterization schemes (e.g.,
85 Fan et al., 2012a; Khain and Lynn, 2009; Khain et al., 2009, 2015; Lebo and Seinfeld, 2011; Lee
86 et al., 2018; Loftus and Cotton, 2014; Wang et al., 2013). Two-moment bulk and bin schemes have
87 been widely used in ACI studies (e.g., Chen et al., 2011; Fan et al., 2013; Khain et al., 2010). In
88 two-moment bulk schemes, hydrometeor size distributions are diagnosed from the predicted
89 number and mass with an assumed spectral shape (e.g., gamma function). The saturation
90 adjustment approach is often used for calculating condensation and evaporation, meaning
91 supersaturation and undersaturation with respect to water are removed in cloud within a timestep.
92 Some bulk schemes take the explicit supersaturation approach to allow supersaturation to evolve
93 (e.g., Morrison and Grabowski, 2007; 2008). In bin schemes, the size distributions of hydrometeors
94 are discretized by a number of size bins and predicted, which represents some aerosol-cloud
95 interaction processes more physically compared with bulk schemes (Fan et al., 2016; Khain et al.,
96 2015). Supersaturation is generally predicted in bin schemes.

97 Many studies have shown that bulk schemes are limited in representing certain important
98 microphysical processes such as aerosol activation, condensation, deposition, sedimentation, and
99 rain evaporation (Ekman et al., 2011; Khain et al., 2009; Lee et al. 2018; Li et al., 2009; Milbrandt

and Yau, 2005; Morrison, 2012; Wang et al., 2013). Though bin cloud microphysics can provide a more rigorous numerical solution and a more robust cloud microphysics representation than typical bulk microphysics, it is often applied in simulations for process understanding but rarely in operational applications due to the expensive computation cost. For not introducing further computation cost, bins schemes are also often run with a prescribed aerosol spectrum assuming a fixed composition and a simple aerosol budget treatment without coupling with chemistry/aerosol calculations. As a result, many aerosol life cycle processes such as aerosol nucleation, growth, aqueous chemistry, aerosol resuspension, and below-cloud wet removal are missing or crudely parameterized. Therefore, it is difficult to simulate the spatial and temporal variabilities of aerosol chemical composition and size distribution. In Gao et al. (2016), we have coupled a spectral-bin microphysics scheme (SBM; Fan et al., 2012a; Khain et al., 2004) with the Chemistry version of Weather Research and Forecast model (WRF-Chem; Grell et al., 2005; Skamarock et al., 2008), called WRF-Chem-SBM, to address above-mentioned limitations. In this new model, the SBM was coupled with the Model for Simulating Aerosol Interactions and Chemistry (MOSAIC; Fast et al., 2006; Zaveri et al., 2008). The newly coupled system was initially evaluated for warm marine stratocumulus clouds and showed a much-improved simulation of cloud droplet number concentration and liquid water content compared with the default Morrison two-moment bulk scheme (Gao et al., 2016).

The Houston area in summer, where isolated convective clouds with very warm cloud-bases often occurred in the afternoon (Yuan et al., 2008), offers (a) a combination of polluted aerosols from the urban and industrial area of Houston with significantly low background aerosol concentrations surrounding Houston, (b) aerosol sources that are not correlated with meteorology, and (c) weak synoptic forcing along with strong local triggering in the form of land-sea contrasts

and sea breeze fronts. This combination allows the manifestation of potentially large aerosol effects. In this study, we choose a sea-breezed induced DCC case occurring 19-20 June 2013 near Houston to (1) evaluate the performances of WRF-Chem-SBM in simulating deep convective clouds and (2) gain a better understanding of the differences in aerosol effects predicted by SBM and the Morrison two-moment bulk scheme as well as the major factors/processes responsible for the differences. Considering that the convective clouds over the Houston area are mainly impacted by the aerosols produced from anthropogenic activities, we focus on the anthropogenic aerosol effect in this study. The simulated storm case is the same as the case for the Aerosol-Cloud-Precipitation-Cloud (ACPC) Model Intercomparison Project (Rosenfeld et al., 2014; www.acpcinitiative.org).

2 Case Description and Observational Data

A local convective event near Houston, Texas on 19-20 June 2013 is selected for the study owing to the most favorable conditions for simulating isolated convective cells. As above-mentioned, the case is also selected for the ACPC Model Intercomparison Project (www.acpcinitiative.org). The isolated relatively weak convective clouds started from the late morning because of a trailing front. With increased solar radiation in the early afternoon and strengthening of a sea breeze circulation that transports warm and humid air from the Gulf of Mexico to Houston urban area, deep convective cells over Houston and Galveston bay areas developed (Fig. 1). The strong convective cell observed near the Houston city was initiated around 2145 UTC (local time 16:45) and developed to its peak precipitation at 2217 UTC based on radar observation (Fig. 1). The maximum reflectivity was more than 55 dBZ. This storm cell lasted for about 1.5 hours.

We used the following observation data for model evaluation. Particulate matter (PM) 2.5 data provided by Texas Commission for Environmental Quality (TCEQ) at https://www.tceq.texas.gov/agency/data/pm25.html are used to evaluate the simulated aerosols near the surface. The data for evaluating cloud base heights and CCN number concentration at cloud base are obtained from the Visible Infrared Imaging Radiometer Suite (VIIRS) retrievals based on the method of Rosenfeld et al., (2016). The 2-m temperature and 10-m winds are from the North American Land Data Assimilation System (NLDAS) with 0.125-deg resolution at https://climatedataguide.ucar.edu/climate-data/nldas-north-american-land-data-assimilation-system. The observed radar reflectivity is used to evaluate the simulated convective system. The radar reflectivity is obtained from Next-Generation Weather Radar (NEXRAD) network at https://www.ncdc.noaa.gov/data-access/radar-data/nexrad-products, with a temporal frequency of every ~ 5 minutes and 1 km horizontal spatial resolution.

3. Model description and experiments

We conducted model simulations using the version of WRF-Chem based on Gao et al. (2016) coupling with the Morrison two-moment scheme (Morrison et al., 2005; Morrison et al., 2009; Morrison and Milbrandt, 2011) and SBM (Khain et al., 2004; Fan et al., 2012). The version of SBM employed in this study is a fast version of the Hebrew University Cloud Model (HUCM) described by Khain et al. (2004) with improvements from Fan et al. (2012a) and (2017). The considered hydrometer size distributions are droplets/raindrops, cloud ice/snow, and graupel. The graupel version is used because it is more appropriate for simulating the convective storm over the Houston area than the hail version. SBM is currently coupled with the four-sector version of MOSAIC (0.039-0.156, 0.156-0.624, 0.624-2.5 and 2.5-10.0 μm). As detailed in Gao et al. (2016), the aerosol processes including aerosol activation, resuspension, and in-cloud wet-removal are also

168 improved. Theoretically, both aerosol and cloud processes can be more realistically simulated
169 particularly under the conditions of complicated aerosol compositions and aerosol spatial
170 heterogeneity compared with original WRF-Chem. The dynamic core of WRF-Chem-SBM is the
171 Advanced Research WRF model that is fully compressible and non-hydrostatic with a terrain-
172 following hydrostatic pressure vertical coordinate (Skamarock et al., 2008). The grid staggering is
173 the Arakawa C-grid. The model uses the Runge-Kutta 3rd order time integration schemes, and the
174 3rd and 5th order advection schemes are selected for the vertical and horizontal directions,
175 respectively. The positive definite option is employed for advection of moist and scalar variables.
176 Two nested domains with horizontal grid spacings of 2 and 0.5 km and horizontal grid points
177 of 450 × 350 and 500 × 400 for Domain 1 and Domain 2, respectively, are used (Fig. 2a), with 51
178 vertical levels up to 50 hPa which allows about 50-100 m grid spacings below 2-km altitude and
179 ~500 m above it. The simulations for Domain 1 and Domain 2 are run separately and the Domain
180 1 simulations serve to provide the chemical and aerosol lateral boundary and initial conditions of
181 Domain 2. The chemical and aerosol lateral boundary and initial conditions for Domain 1
182 simulations were from a quasi-global WRF-Chem simulation at 1-degree grid spacing, and
183 meteorological lateral boundary and initial conditions were created from MERRA-2 at the grid
184 spacing of 0.5° × 0.625° (Gelaro et al., 2017). Two simulations were run over Domain 1 with
185 anthropogenic emissions turned on and off, respectively, to provide two different aerosol scenarios
186 for the initial and boundary chemical and aerosol conditions for Domain 2 simulations: (1) a
187 polluted aerosol scenario with anthropogenic aerosols accounted which is for the real situation; (2)
188 an assumptive clean scenario without anthropogenic aerosols. Domain 2 is run with initial and
189 lateral boundary chemical and aerosols fields from Domain 1 outputs and initial and lateral
190 boundary meteorological conditions from MERRA-2. Note that we use the meteorology from

MERRA-2 as the initial and lateral boundary conditions for Domain 2 instead of Domain 1 outputs, because we want to keep the initial and lateral boundary meteorological conditions the same for all the sensitivity tests with different microphysics and aerosol setups (meteorology is different between the two simulations over Domain 1).

The simulations in Domain 1 were initiated at 0000 UTC on 14 Jun and ended at 1200 UTC 20 June with about 5 days for the chemistry spin-up. The meteorological field was reinitialized every 36 hours to prevent the model drifting. The dynamic time step was 6 s for Domain 1 and 3 s for Domain 2. The anthropogenic emission was from NEI-2011 emissions. The biogenic emission came from the Model of Emissions of Gases and Aerosols from Nature (MEGAN) product (Guenther et al., 2006). The biomass burning emission was from the Fire Inventory from NCAR (FINN) model (Wiedinmyer et al., 2011). We used the Carbon Bond Mechanism Z (CBMZ) gas-phase chemistry (Zaveri and Peters, 1999) and MOSAIC aerosol model with four bins (Zaveri et al., 2008). The physics schemes other than microphysics applied in the simulation are the Unified Noah land surface scheme (Chen and Dudhia, 2001), Mellor-Yamada-Janjic planetary boundary layer scheme (Janjic et al., 1994), Multi-layer, Building Environment Parameterization (BEP) urban physics scheme (Salamanca and Martilli, 2010), the RRTMG longwave and shortwave radiation schemes (Iacono et al., 2008).

The main purpose of the simulations in Domain 1 is to provide initial and boundary chemical and aerosol conditions for the simulations in Domain 2. To save computational cost, WRF-Chem coupled with Morrison two-moment bulk microphysics scheme (Morrison et al., 2005) is used for the simulations in Domain 1. Two simulations run for Domain 1 are referred to as D1_MOR_anth in which the anthropogenic emissions are turned on and D1_MOR_noanth where the anthropogenic emissions are turned off. Then four major experiments are carried out to simulate

214 the convective event near Houston over Domain 2 with two cloud microphysics schemes and two
215 aerosol scenarios, respectively. We refer to the simulation in which SBM is used and the
216 anthropogenic emissions are included using the initial and boundary chemicals and aerosols from
217 D1_MOR_anth, as our baseline simulation (referred to as "SBM_anth"). SBM_noanth is based on
218 SBM_anth but uses initial and boundary chemicals and aerosols from D1_MOR_noanth and turns
219 off the anthropogenic emissions, meaning that anthropogenic aerosols are not taken into account.
220 MOR_anth and MOR_noanth are the two corresponding simulations to SBM_anth and
221 SBM_noanth, respectively, using the Morrison two-moment bulk microphysics scheme. To
222 examine the contribution of the saturation adjustment approach for condensation and evaporation
223 to the simulated aerosol effects with the Morrison scheme, we further conducted two sensitivity
224 tests, based on MOR_anth and MOR_noanth, by replacing the saturation adjustment approach in
225 the Morrison scheme with the condensation and evaporation calculation based on an explicit
226 representation of supersaturation over a time step as described in Lebo et al. (2012). That is the
227 supersaturation is solved by the source and sink terms of dynamic forcing and
228 condensation/evaporation within a one-timestep. Note in both SBM and this modified Morrison
229 schemes, the supersaturation for condensation and evaporation is calculated after the advection.
230 These two simulations are referred to as MOR_SS_anth and MOR_SS_noanth, respectively. To
231 present more robust results, we carry out a small number of ensembles (three) for each case over
232 Domain 2 (we do not have computer time to do more ensemble runs). The three ensemble runs are
233 only different in the initialization time: 0000 UTC, 0600 UTC, and 1200 UTC on 19 June. All the
234 simulations end at 1200 UTC 20 June. The analysis results for Domain 2 simulations in this study
235 are based on the mean values of three ensemble runs and the ensemble spread is shown as the
236 shaded area in all profile figures.

We evaluate the aerosol and CCN properties simulated by D1_MOR_anth to ensure realistic aerosol fields, which are used for the Domain 2 simulations with anthropogenic aerosols considered. These evaluations are included in section 4.1.

From D1_MOR_anth, we see a very large spatial variability of aerosol number concentrations (Fig. 2b). There are three regions with significantly different aerosol loadings over the domain as shown by the black boxes in Fig. 2b: (a) the Houston urban area, (b) the rural area about 100 km northeast to Houston, and (c) Gulf of Mexico. Aerosols over the Houston urban area are mainly contributed by organic aerosols, which are highly related to industrial and ship channel emissions. The rural area aerosols are mainly from sulfate and sea salt aerosol is the major contributor over the Gulf of Mexico. This suggests that aerosol properties are extremely heterogenous in this region. The aerosols over Houston urban area are generally about 5 and 10 times higher than the rural and Gulf area, respectively (Fig. 2c). The size distributions show a three-mode distribution with the largest differences from the Aitken mode (peaks at 50 nm; Fig. 2c). These ultrafine aerosol particles are mainly contributed by anthropogenic activities (Fig. 2b, d). With the anthropogenic emissions turned off, the simulated aerosols are much lower and have much less spatial variability (Fig. 2d).

4 Result

4.1 Model Evaluation

We first show the evaluation of the aerosol and CCN properties simulated by D1_MOR_anth, which runs over Domain 1, much larger than Domain 2. As described in Table 1, there are eight PM monitoring sites from TCEQ around the Houston area. Surface PM2.5 shows high concentrations at Houston and its downwind regions (Fig. 3). Though not exactly the same,

the values from D1_MOR_anth show a similar distribution with the observations in terms of the surface PM2.5 averaged over 24 hours (the day before the convection near Houston). The hourly variations of ground-level PM2.5 concentrations from both observation and D1_MOR_anth for these sites in the day before the convective initiation is depicted in Fig. 4. Generally, the simulated hourly pattern agrees with the observation for eight stations. D1_MOR_anth reproduces the diurnal variations, especially the increasing trend from 1200 UTC to 1800 UTC 19 Jun prior to the initiation of deep convective cells over Houston and Galveston bay areas.

The evaluation of the cloud base heights and CCN at cloud bases at the warm cloud stage before transitioning to deep clouds (2000 UTC) are shown in Fig.5. Over the Houston and its surrounding area (black box in Fig. 5), the simulated cloud base heights are about 1.5-2 km, in an agreement with the retrieved values from VIIRS satellite, which are around 1.2-1.8 km (Fig. 5a-b). The retrieved CCN concentrations at cloud bases vary significantly over the domain and this spatial variability is generally captured by the model (Fig. 5c-d). For example, D1_MOR_anth simulates some high CCN concentrations (400-800 cm^{-3} with some above 1000 cm^{-3}) over the Houston and around the Bay area, relatively low CCN values at the rural areas (about 200-600 cm^{-3}), and very low values over the Gulf of Mexico (less than 200 cm^{-3}), as shown in Fig. 5d. This is consistent with the spatial variability from the retrievals (Fig. 5c). The evaluation of aerosol properties before the initiation of Houston convective cells and CCN at the warm cloud stage before transitioning to deep clouds provides us confidence in using the chemical and aerosol fields from Domain 1 outputs to feed Domain 2 simulations.

Now we are evaluating near-surface temperature and winds, reflectivity and precipitation simulated by SBM_anth and MOR_anth. Fig. 6 shows the comparisons in 2-m temperature and 10-m winds at 1800 UTC (before the convective initiation). Compared with the coarse resolution

NLDAS data, both SBM_anth and MOR_anth capture the general temperature pattern with a little overestimation at the northeast part of the domain (mainly rural area). The modeled southerly winds do not reach further north as the NLDAS data, possibly because of the feedback of the small-scale features which are simulated with the high resolution to mesoscale circulations. However, the simulation of temperature over Houston and sea breeze winds from the Gulf of Mexico to Houston is the most important in this case. SBM_anth predicts a slightly higher temperature than MOR_anth in the northern part of the Houston region (purple box in Fig. 6), which agrees with NLDAS better. SBM_anth gets the similar southerly winds from the Gulf of Mexico to Houston as shown in NLDAS, while the southerly winds from Gulf of Mexico become very weak or disappear prior to reaching Houston in MOR_anth.

For the Houston convective cell that we focused (red box in Fig. 7a), SBM_anth simulates it well in both location and high reflectivity value (greater than 50 dBZ) in comparison with the NEXRAD observation (Fig. 7a-b). The simulated composite reflectivities (i.e., the column maximum) are up to 55-60 dBZ from all three ensemble members, consistent with NEXRAD. With the Morrison scheme, MOR_anth simulates several small convective cells near Houston with a maximum reflectivity of 55 dBZ or less (Fig. 7c). All three ensemble members consistently show smaller but more scattered convective cells with the Morrison scheme compared with SBM. The contoured frequency by altitude diagram (CFAD) plots for the entire storm period show that SBM_anth is in a better agreement with observation compared with MOR_anth, especially for the vertical structure of the high reflectivity range (greater than 48 dBZ, black dashed lines in Fig. 8) and echo top heights, which can reach up to 14-15 km (Fig. 8a-b). MOR_anth overestimates the occurrence frequencies of the 35-45 dBZ range and underestimates those of the low and high

304 reflectivity ranges (less than 15 dBZ or larger than 50 dBZ) as well as the echo top heights (1-2
305 km lower than SBM_anth; Fig. 8c).

306 For the precipitation rates averaged over the study area (red box in Fig. 7), the observation
307 shows two peaks, which are captured by both SBM_anth and MOR_anth (Fig. 9a). However, the
308 timing for the first peak is about 30 and 60 min earlier in SBM_anth and MOR_anth than the
309 observation, respectively. Also, SBM_anth predicts the rain rate intensities at the two peak times
310 more consistent with the observations whereas MOR_anth underestimates the rain rate intensity at
311 the second peak time (Fig. 9a). The large precipitation rates (greater than 15 mm h^{-1}) in SBM_anth
312 has a ~1.5 times larger occurrence probability than those in MOR_anth, showing a better
313 agreement with the observation (Fig. 9b). The observed accumulated rain over the time period
314 shown in Fig. 9a is about 3.8 mm, both SBM_anth (~4.5 mm) and MOR_anth (~4.2 mm)
315 overestimate the accumulated precipitation due to the longer rain period compared with the
316 observations. Overall, the performance of SBM_anth is superior to MOR_anth in simulating the
317 location and intensity of the convective storm and associated precipitation.

318 **4.2 Simulated Aerosol Effects on Cloud and Precipitation**

319 Now we look at the effects of anthropogenic aerosols on the deep convective storm
320 simulated with SBM and Morrison microphysics schemes. Fig. 9a shows that with the SBM
321 scheme, anthropogenic aerosols remarkably increase the mean surface rain rates (by ~30%; from
322 SBM_noanth to SBM_anth), mainly because of the increased occurrence frequency (nearly
323 doubled) for relatively large rain rates (i.e., 10-15 mm h^{-1} and >15 mm h^{-1}) in Fig. 9b. With the
324 Morrison scheme, the changes in mean precipitation and the PDF from MOR_noanth to
325 MOR_anth are relatively small, showing a very limited aerosol effect on precipitation. With the
326 SBM scheme, the increase in the updraft speeds by the anthropogenic aerosols is even more notable

than the precipitation (Fig. 10a-b). Above 5-km altitude, the occurrence frequencies of updraft speed greater than 0.4% extend to much larger values, with 36 m s^{-1} at the upper levels in SBM_anth while only ~ 20 m s^{-1} in SBM_noanth. With the Morrison scheme, the changes are not significant by the anthropogenic aerosols (MOR_noanth vs MOR_anth in Fig. 10c-d). From MOR_noanth to MOR_anth, there is a slight increase in updraft speed at around 9-11 km altitudes but a slight decrease at 6-8 km altitudes. The significant invigoration of convective intensity by anthropogenic aerosols with the SBM scheme explains the much larger occurrences of relatively large rain rates and overall more surface precipitation due to the anthropogenic aerosol effect (Fig. 9). Note Fig. 9a shows that anthropogenic aerosols lead to an earlier start of the precipitation with both SBM and Morrison, which reflects the faster transition of warm rain to mixed-phase precipitation. We do see the delay of warm rain by aerosols but only about 5 min (probably due to the humid condition of the case), which is difficult to be shown in Fig. 9a since averaged rain rate for the analysis box is ~0.02 mm hr^{-1} and the time period is very short (~10 min).

Now the question is why the anthropogenic aerosols enhance the convective intensity of the storm with the SBM scheme while the effect is very small with the Morrison scheme. Fig. 11 shows the vertical profiles of mean updraft velocity, thermal buoyancy (from temperature and moisture perturbation), and total latent heating rate of the top 25th percentile updrafts with a value greater than 2 m s^{-1} during the deep convective cloud stage. With the SBM microphysics scheme, the increased convective intensity due to the anthropogenic aerosol effect corresponds to the increased thermal buoyancy which is particularly notable at upper levels (~ 20%) from SBM_noanth to SBM_anth (Fig. 11a, c). The increased thermal buoyancy can be explained by the increased total latent heating (Fig. 11e), which is mainly from the larger condensation latent heating (Fig. 12a). From SBM_noanth to SBM_anth, the latent heating from ice-related

microphysical processes (including deposition, drop freezing, and riming) has a relatively smaller increase than that from condensation (about half of the increase in condensation latent heating as shown in Fig. 12a). As shown in Fan et al., (2018), the increase in lower-level condensation latent heating has a much larger effect on intensifying updraft intensity compared with the same amount of increase in high-level latent heating from ice-related microphysical processes. This suggests that the convective invigoration by the anthropogenic aerosols with the SBM scheme should be mainly through the "warm-phase invigoration" mechanism. Compared with the Morrison scheme, the increase of total latent heating by the anthropogenic aerosols is almost doubled with the SBM scheme, explaining more remarkable enhancement of thermal buoyancy and thus the convective intensity (red lines vs blue lines in Fig. 11). From MOR_noanth to MOR_anth, there is a small increase in both the condensation latent heating and high-level latent heating associated with ice-related processes (blue lines in Fig. 12b). The major difference in the increase of latent heating by the anthropogenic aerosols between SBM and Morrison microphysics schemes comes from the condensation latent heating, with a ~20% increase with SBM but only ~ 8% with Morrison (Fig. 12). The lack of a significant increase in condensation latent heating limits the "warm-phase invigoration", mainly responsible for the limited aerosol impacts on the convective intensity and associated precipitation with the Morrison scheme.

To understand why the responses of condensation to the anthropogenic aerosols are different between the SBM and Morrison schemes, we look into the process rates of drop nucleation and condensation (Fig. 13). The calculations of aerosol activation and condensation/evaporation in the SBM scheme are based on the Köhler theory and diffusional growth equations in light of particle size and supersaturation, receptively. Whereas in the Morrison scheme, the Abdul-Razzak and Ghan (2002) parameterization is used for aerosol activation and

the saturation adjustment method is applied for condensation and evaporation calculation. With the SBM scheme, the anthropogenic aerosols increase the drop nucleation rates by a few times over the profile (red lines in Fig. 13a), and the condensation rates are also drastically increased (doubled between 4-6 km altitudes as shown in Fig. 13c). The enhanced condensation rate by the anthropogenic aerosols is because much more aerosols are activated to form a larger number of small droplets, increasing the integrated droplet surface area for condensation, as documented in Fan et al., (2018). As a result, supersaturation is drastically lower in SBM_anth than SBM_noanth (green lines in Fig. 13a). With the Morrison scheme, we still see a large increase in the droplet nucleation rate (Fig. 13b). However, the condensation rates are barely increased (blue solid vs. dashed lines in Fig. 13d). We hypothesize that the lack of response of condensation to the increased aerosol activation with the Morrison scheme is mainly because of the saturation adjustment calculation of the condensation and evaporation process. The approach does not allow supersaturation in cloud and the calculation does not depend on supersaturation, thus removes the sensitivity to the anthropogenic aerosols.

To verify our hypothesis and examine how much the saturation adjustment method is responsible for the weak responses of condensation latent heating and convection to the added anthropogenic aerosols, we conducted two additional sensitivity tests by replacing the saturation adjustment approach in the Morrison scheme with the condensation and evaporation calculation based on an explicit representation of supersaturation over a time step, as described in Section 3. The result shows the Morrison scheme with the simple calculation of supersaturation for condensational growth significantly changes the condensation rate (orange vs. blue lines in Fig. 13d) and a similarly large enhancement (from MOR_SS_noanth to MOR_SS_anth in Fig. 13d) is seen as the SBM scheme (Fig. 13c). This leads to a larger increase in condensation latent heating

396 (orange lines in Figure 12b) compared with the original Morrison scheme, resulting in a similarly
397 large increase in thermal buoyancy by the anthropogenic aerosols as with the SBM scheme(orange
398 lines in Fig. 11d), thus a similarly large increase in the convective intensity (orange lines in Fig.
399 11b). The increase of precipitation from MOR_SS_noanth to MOR_SS_anth is also similar to that
400 with the SBM scheme (not shown). These results verify that the saturation adjustment approach
401 for parameterizing condensation and evaporation is the major reason responsible for limited
402 aerosol effects on convective intensity and precipitation with the Morrison scheme. Past studies
403 also showed the limitations of the saturation adjustment approach in simulating aerosol impacts
404 on deep convective clouds (e.g., Fan et al., 2016; Lebo et al., 2012; Lee et al., 2018; Wang et al.,
405 2013).

406 Fig. 14 and Fig. 15 show the responses of hydrometeor mass and number to anthropogenic
407 aerosol effects. With the SBM scheme, the increases in mass and number of cloud droplets,
408 raindrops, and total ice particles (ice, snow, and graupel) by the anthropogenic aerosols are very
409 significant (Fig. 14-15, left), corresponding to convective invigoration. The increase of the total
410 ice mass is particularly significant (from 3.5 to 5.5 g kg^{-1} around 10-km altitude), suggesting a
411 large effect of enhanced convective intensity on ice hydrometeors. However, with the Morrison
412 scheme, little change is seen (Fig. 14-15, right, blue lines). By replacing the saturation adjustment
413 with a simple calculation based on supersaturation for condensation and evaporation in the
414 Morrison scheme, the increases in those hydrometeor masses become as evident as those with the
415 SBM scheme (Fig. 14-15, right, orange lines).

416 Now we explain why the saturation adjustment approach leads to smaller condensational
417 heating than the explicit supersaturation approach in Morrison Scheme and why it leads to a
418 smaller sensitivity to aerosols compared with the explicit supersaturation approach. We examine

419 the time evolution of latent heating, updraft, and hydrometeor properties. At the warm cloud stage
420 at 1700 UTC, the saturation adjustment indeed produces more condensational latent heating which
421 leads to larger buoyancy and stronger updraft intensity compared to the explicit supersaturation
422 because of removing supersaturation (Fig. 16, left, blue vs. orange). By the time of 1900 UTC
423 when the clouds have developed into mixed-phase clouds, the saturation adjustment produces less
424 condensational heating and weaker convection than the explicit supersaturation approach (Fig. 16,
425 middle). The results remain similarly later at the deep cloud stage 2100 UTC (Fig. 16, right).
426 How does this change happen from 1700 to 1900 UTC? At the warm cloud stage (17:00
427 UTC), the saturation adjustment produces droplets with larger sizes (up to 100% larger for the
428 mean radius) than the explicit supersaturation because of more cloud water produced as a result of
429 zeroing-out supersaturation at each time step (droplet formation is similar between the two cases
430 as shown in Fig. 13). This results in much faster and larger warm rain, while with the explicit
431 supersaturation rain number and mass are absent at 1700 UTC as shown in Fig. 17d and 18d). As
432 a result, when evolving into the mixed-phase stage (19:00 UTC), much fewer cloud droplets are
433 transported to the levels above the freezing level (Fig. 17b and 18b). Whereas with the explicit
434 supersaturation, because of the delayed/suppressed warm rain and smaller droplets (the mean
435 radius is decreased from 8 to 6 μm at 3 km), much more cloud droplets are lifted to the higher
436 levels. Correspondingly, a few times higher total ice particle number and mass are seen compared
437 with the saturation adjustment (Fig. 17g and 18g) because more droplets above the freezing level
438 induce stronger ice processes (droplet freezing, riming, and deposition). This leads to more latent
439 heat release (Fig. 16e), which increases the buoyancy and convective intensity. With the explicit
440 supersaturation, increasing aerosols leads to a larger reduction in droplet size (up to 1 μm more in
441 the mean radius) than the saturation adjustment, therefore more enhanced ice microphysical

processes and the larger latent heat. Besides, the condensational heating is more enhanced by aerosols with the explicit supersaturation (Fig. 16). Together, a much larger sensitivity to aerosols is seen with the explicit supersaturation.

5 Conclusions and Discussion

We have conducted model simulations of a deep convective cloud case occurring on 19 June 2013 over the Houston area with WRF-Chem coupled with the SBM and Morrison microphysics schemes to (1) evaluate the performance of WRF-Chem-SBM in simulating the deep convective clouds, and (2) explore the differences in aerosol effects on the deep convective clouds produced by the SBM and Morrison schemes and the major factors responsible for the differences.

We have evaluated the simulated aerosols, CCN, cloud base heights, reflectivity, and precipitation. The model simulates the large spatial variability of aerosols and CCN from the Gulf of Mexico, rural areas, to Houston city. On the bulk magnitudes, the model captures the surface PM2.5, cloud base height, and CCN at cloud bases near the Houston reasonably well. These realistically simulated aerosol fields were fed to higher resolution simulations (0.5 km) using the SBM and Morrison schemes. With the SBM scheme, the model simulates a deep convective cloud over Houston in a better agreement with the observed radar reflectivity and precipitation, compared with using the Morrison scheme.

By excluding the anthropogenic aerosols in the simulations, the effects of anthropogenic aerosols on the deep convective clouds and differences in aerosol effects using the two microphysics schemes were examined. With the SBM scheme, anthropogenic aerosols notably increase the convective intensity, enhance the peak precipitation rate over the Houston area (by ~ 30%), and double the frequencies of relatively large rain rates (> 10 mm h^{-1}). The enhanced convective intensity by anthropogenic aerosols makes the simulated storm agree better with the

observed, mainly attributed to the increased condensation latent heating, indicating the "warm-phase invigoration". In contrast, with the Morrison scheme, there is no significant anthropogenic aerosol effect on the convective intensity and precipitation.

Sensitivity tests by replacing the saturation adjustment with the condensation and evaporation calculation based on an explicit supersaturation approach show weaker warm clouds with smaller cloud droplet sizes because of smaller condensational growth than the saturation adjustment which eliminates all supersaturation. This leads to less efficient conversion of cloud droplet to rain and allows more cloud droplets to be transported to altitudes above the freezing level at the mixed-phase and deep cloud stages, resulting in stronger ice microphysical processes (freezing, riming, and deposition), therefore larger latent heat release, invigorating convective updrafts. Lebo et al. (2012) showed a similar feature that the saturation adjustment has larger total condensate mass at the beginning but less at the later stage compared to the explicit supersaturation approach, particularly in total ice mass. Grabowski and Morrison (2017) also showed that the saturation adjustment affected ice processes by producing larger ice particles with larger falling velocities compared with the explicit supersaturation approach, leading to the reduction of anvil clouds. The increased condensation is significant for the enhanced warm clouds when saturation adjustment is used. This is different from the points of Grabowski and Jarecka (2015) that the cloud edge evaporation effect is more important for the nonprecipitating shallow clouds.

It is also notable that the adjusted Morrison scheme by replacing saturation adjustment with explicit supersaturation for condensation and evaporation show the similar aerosol effects on condensation, convective intensity, hydrometeor mass mixing ratios, and precipitation as with the SBM scheme. Therefore, the saturation adjustment method for the condensation and evaporation calculation is mainly responsible for the limited aerosol effects with the Morrison scheme. This is

because the saturation adjustment method does not allow for the "warm-phase invigoration", which is different from Lebo et al. (2012) showing that the saturation adjustment artificially enhanced condensation latent heating at low levels and limited the potential for aerosols to invigorate convection through the "cold-phase invigoration" mechanism in their idealized simulations of a supercell storm with the thermal bubble initiation. In this study of the thunderstorm with WRF real-case simulations for both chemistry/aerosols and clouds, the saturation adjustment method actually leads to a smaller condensation latent heating than the explicit calculation with supersaturation (solid bold blue vs. solid bold orange line in Fig. 12b). Thus, when the computational resource is not sufficient or in other situations such as the application of SBM is not available, the Morrison scheme modified with the condensation and evaporation calculation based on a simple representation of supersaturation can be applied to study aerosol effects on convective clouds, especially for warm and humid cloud cases in which the response of condensation to aerosols is particularly important.

Following Fan et al., (2018), which showed that the "warm-phase invigoration" mechanism was manifested by ultrafine aerosol particles in the Amazon warm and humid environment with extremely low background aerosol particles. Here we showed that in summer anthropogenic aerosols over the Houston area may also enhance the thunderstorm intensity and precipitation through the same mechanism by secondary nucleation of numerous ultrafine aerosol particles from the anthropogenic sources. But the magnitude of the effect is not as substantial as in the Amazon environment. Possible reasons include that background aerosols are much higher over the Houston area and air is not as humid as Amazon.

Acknowledgments

This study is supported by the U.S. Department of Energy Office of Science through its Early Career Award Program and a grant DE-SC0018996 and the NSF (AGS1837811). PNNL is operated for the US Department of Energy (DOE) by Battelle Memorial Institute under Contract DE-AC05-76RL01830. This research used resources of PNNL Institutional Computing (PIC), and the National Energy Research Scientific Computing Center (NERSC), a U.S. Department of Energy Office of Science User Facility operated under contract DE-AC02-05CH11231. We thank Chun Zhao at China University of Science and Technology for providing the quasi-global WRF-Chem simulation data, and Hugh Morrison at the National Center for Atmospheric Research for the Morrison code with supersaturation-forced condensation and evaporation calculation.

Reference

Abdul-Razzak, H., and Ghan, S. J.: A parameterization of aerosol activation - 3. Sectional representation, J Geophys Res-Atmos, 107, 4026, doi: 10.1029/2001jd000483, 2002.

Andreae, M. O., Jones, C. D., and Cox, P. M.: Strong present-day aerosol cooling implies a hot future, Nature, 435, 1187-1190, doi: 10.1038/nature03671, 2005.

Arakawa, A.: The cumulus parameterization problem: Past, present, and future, J Climate, 17, 2493-2525, doi: 10.1175/1520-0442(2004)017<2493:Ratcpp>2.0.Co;2, 2004.

Chen, F., and Dudhia, J.: Coupling an advanced land surface-hydrology model with the Penn State-NCAR MM5 modeling system. Part I: Model implementation and sensitivity, Mon Weather Rev, 129, 569-585, doi: 10.1175/1520-0493(2001)129<0569:Caalsh>2.0.Co;2, 2001.

Chen Q., J. Fan, Y. Yin, and B. Han: Aerosol impacts on mesoscale convective systems forming under different vertical wind shear conditions. Journal of Geophysical Research: Atmospheres, 125, e2018JD030027, 2020.

Chen, Y. C., Xue, L., Lebo, Z. J., Wang, H., Rasmussen, R. M., and Seinfeld, J. H.: A comprehensive numerical study of aerosol-cloud-precipitation interactions in marine stratocumulus, Atmos Chem Phys, 11, 9749-9769, doi: 10.5194/acp-11-9749-2011, 2011.

Dagan, G., Koren, I., Altaratz, O. and Lehahn, Y.: Shallow convective cloud field lifetime as a key factor for evaluating aerosol effects. iScience, 10, 192–202, 2018.

Ekman, A. M. L., Engstrom, A., and Soderberg, A.: Impact of Two-Way Aerosol-Cloud Interaction and Changes in Aerosol Size Distribution on Simulated Aerosol-Induced Deep Convective Cloud Sensitivity, J Atmos Sci, 68, 685-698, doi: 10.1175/2010jas3651.1, 2011.

544 Fan, J. W., Zhang, R. Y., Li, G. H., and Tao, W. K.: Effects of aerosols and relative humidity on
545 cumulus clouds, J Geophys Res-Atmos, 112, D14204, doi: 10.1029/2006jd008136, 2007.
546 Fan, J. W., Yuan, T. L., Comstock, J. M., Ghan, S., Khain, A., Leung, L. R., Li, Z. Q., Martins, V.
547 J., and Ovchinnikov, M.: Dominant role by vertical wind shear in regulating aerosol effects
548 on deep convective clouds, J Geophys Res-Atmos, 114, D22206, doi:
549 10.1029/2009jd012352, 2009.
550 Fan, J. W., Leung, L. R., Li, Z. Q., Morrison, H., Chen, H. B., Zhou, Y. Q., Qian, Y., and Wang,
551 Y.: Aerosol impacts on clouds and precipitation in eastern China: Results from bin and
552 bulk microphysics, J Geophys Res-Atmos, 117, D00k36, doi: 10.1029/2011jd016537,
553 2012a.
554 Fan, J. W., Rosenfeld, D., Ding, Y. N., Leung, L. R., and Li, Z. Q.: Potential aerosol indirect effects
555 on atmospheric circulation and radiative forcing through deep convection, Geophys Res
556 Lett, 39, L09806, doi: 10.1029/2012gl051851, 2012b.
557 Fan, J. W., Leung, L. R., Rosenfeld, D., Chen, Q., Li, Z. Q., Zhang, J. Q., and Yan, H. R.:
558 Microphysical effects determine macrophysical response for aerosol impacts on deep
559 convective clouds, P Natl Acad Sci USA, 110, E4581-E4590, doi:
560 10.1073/pnas.1316830110, 2013.
561 Fan, J. W., Wang, Y., Rosenfeld, D., and Liu, X. H.: Review of Aerosol-Cloud Interactions:
562 Mechanisms, Significance, and Challenges, J Atmos Sci, 73, 4221-4252, doi: 10.1175/Jas-
563 D-16-0037.1, 2016.
564 Fan, J. W., Han, B., Varble, A., Morrison, H., North, K., Kollias, P., Chen, B. J., Dong, X. Q.,
565 Giangrande, S. E., Khain, A., Lin, Y., Mansell, E., Milbrandt, J. A., Stenz, R., Thompson,
566 G., and Wang, Y.: Cloud-resolving model intercomparison of an MC3E squall line case:

Part I-Convective updrafts, J Geophys Res-Atmos, 122, 9351-9378, doi: 10.1002/2017jd026622, 2017.

Fan, J. W., Rosenfeld, D., Zhang, Y. W., Giangrande, S. E., Li, Z. Q., Machado, L. A. T., Martin, S. T., Yang, Y., Wang, J., Artaxo, P., Barbosa, H. M. J., Braga, R. C., Comstock, J. M., Feng, Z., Gao, W. H., Gomes, H. B., Mei, F., Pohlker, C., Pohlker, M. L., Poschl, U., and de Souza, R. A. F.: Substantial convection and precipitation enhancements by ultrafine aerosol particles, Science, 359, 411-418, doi: 10.1126/science.aan8461, 2018.

Fast, J. D., Gustafson, W. I., Easter, R. C., Zaveri, R. A., Barnard, J. C., Chapman, E. G., Grell, G. A., and Peckham, S. E.: Evolution of ozone, particulates, and aerosol direct radiative forcing in the vicinity of Houston using a fully coupled meteorology-chemistry-aerosol model, J Geophys Res-Atmos, 111, D21305, doi: 10.1029/2005jd006721, 2006.

Gao, W. H., Fan, J. W., Easter, R. C., Yang, Q., Zhao, C., and Ghan, S. J.: Coupling spectral-bin cloud microphysics with the MOSAIC aerosol model in WRF-Chem: Methodology and results for marine stratocumulus clouds, J Adv Model Earth Sy, 8, 1289-1309, doi: 10.1002/2016ms000676, 2016.

Gelaro, R., McCarty, W., Suarez, M. J., Todling, R., Molod, A., Takacs, L., Randles, C. A., Darmenov, A., Bosilovich, M. G., Reichle, R., Wargan, K., Coy, L., Cullather, R., Draper, C., Akella, S., Buchard, V., Conaty, A., da Silva, A. M., Gu, W., Kim, G. K., Koster, R., Lucchesi, R., Merkova, D., Nielsen, J. E., Partyka, G., Pawson, S., Putman, W., Rienecker, M., Schubert, S. D., Sienkiewicz, M., and Zhao, B.: The Modern-Era Retrospective Analysis for Research and Applications, Version 2 (MERRA-2), J Climate, 30, 5419-5454, doi: 10.1175/Jcli-D-16-0758.1, 2017.

589 Grabowski, W. W., and D.Jarecka: Modeling condensation in shallow nonprecipitating
590 convection. J. Atmos. Sci., 72, 4661–4679, 2015.
591 Grabowski, W. W., and H.Morrison: Untangling microphysical impacts on deep convection
592 applying a novel modeling methodology. Part II: Double-moment microphysics. J. Atmos.
593 Sci., 73, 3749–3770, 2016.
594 Grabowski, W. W., and H. Morrison: Modeling condensation in deep convection, J. Atmos.
595 Sci., 74, 2247– 2267, doi:10.1175/JAS-D-16-0255.1, 2017.
596 Grabowski, W. W., and H. Morrison: Do ultrafine cloud condensation nuclei invigorate deep
597 convection? J. Atmos. Sci., 77(7), 2567-2583, doi: 10.1175/JAS-D-20-0012.1, 2020.
598 Grell, G. A., Peckham, S. E., Schmitz, R., McKeen, S. A., Frost, G., Skamarock, W. C., and Eder,
599 B.: Fully coupled "online" chemistry within the WRF model, Atmos Environ, 39, 6957-
600 6975, doi: 10.1016/j.atmosenv.2005.04.027, 2005.
601 Guenther, A., Karl, T., Harley, P., Wiedinmyer, C., Palmer, P. I., and Geron, C.: Estimates of
602 global terrestrial isoprene emissions using MEGAN (Model of Emissions of Gases and
603 Aerosols from Nature), Atmos Chem Phys, 6, 3181-3210, doi: 10.5194/acp-6-3181-2006,
604 2006.
605 Haywood, J., and Boucher, O.: Estimates of the direct and indirect radiative forcing due to
606 tropospheric aerosols: A review, Rev Geophys, 38, 513-543, doi: 10.1029/1999rg000078,
607 2000.
608 Houze, R. A.: Cloud dynamics, 2. edn., Elsevier/Acad. Press, Amsterdam, 2014.
609 Iacono, M. J., Delamere, J. S., Mlawer, E. J., Shephard, M. W., Clough, S. A., and Collins, W. D.:
610 Radiative forcing by long-lived greenhouse gases: Calculations with the AER radiative
611 transfer models, J Geophys Res-Atmos, 113, D13103, doi: 10.1029/2008jd009944, 2008.

612 Janjic, Z. I.: The Step-Mountain Eta Coordinate Model - Further Developments of the Convection,
613 Viscous Sublayer, and Turbulence Closure Schemes, Mon Weather Rev, 122, 927-945, doi:
614 10.1175/1520-0493(1994)122<0927:Tsmecm>2.0.Co;2, 1994.
615 Khain, A., Pokrovsky, A., Pinsky, M., Seifert, A., and Phillips, V.: Simulation of effects of
616 atmospheric aerosols on deep turbulent convective clouds using a spectral microphysics
617 mixed-phase cumulus cloud model. Part I: Model description and possible applications, J
618 Atmos Sci, 61, 2963-2982, doi: 10.1175/Jas-3350.1, 2004.
619 Khain, A., Rosenfeld, D., and Pokrovsky, A.: Aerosol impact on the dynamics and microphysics
620 of deep convective clouds, Q J Roy Meteor Soc, 131, 2639-2663, doi: 10.1256/qj.04.62,
621 2005.
622 Khain, A., and Lynn, B.: Simulation of a supercell storm in clean and dirty atmosphere using
623 weather research and forecast model with spectral bin microphysics, J Geophys Res-Atmos,
624 114, D19209, doi: 10.1029/2009jd011827, 2009.
625 Khain, A., Lynn, B., and Dudhia, J.: Aerosol Effects on Intensity of Landfalling Hurricanes as
626 Seen from Simulations with the WRF Model with Spectral Bin Microphysics, J Atmos Sci,
627 67, 365-384, doi: 10.1175/2009jas3210.1, 2010.
628 Khain, A. P., BenMoshe, N., and Pokrovsky, A.: Factors determining the impact of aerosols on
629 surface precipitation from clouds: An attempt at classification, J Atmos Sci, 65, 1721-1748,
630 doi: 10.1175/2007jas2515.1, 2008.
631 Khain, A. P., Leung, L. R., Lynn, B., and Ghan, S.: Effects of aerosols on the dynamics and
632 microphysics of squall lines simulated by spectral bin and bulk parameterization schemes,
633 J Geophys Res-Atmos, 114, D22203, doi: 10.1029/2009jd011902, 2009.

634 Khain, A. P., Beheng, K. D., Heymsfield, A., Korolev, A., Krichak, S. O., Levin, Z., Pinsky, M.,
635 Phillips, V., Prabhakaran, T., Teller, A., van den Heever, S. C., and Yano, J. I.:
636 Representation of microphysical processes in cloud-resolving models: Spectral (bin)
637 microphysics versus bulk parameterization, Rev Geophys, 53, 247-322, doi:
638 10.1002/2014rg000468, 2015.
639 Koren, I., Dagan, G., and Altaratz, O.: From aerosol-limited to invigoration of warm convective
640 clouds, Science, 344, 1143-1146, doi: 10.1126/science.1252595, 2014.
641 Korolev A., and I. Mazin: Supersaturation of water vapor in clouds. J. Atmos. Sci., 60, 2957-2974,
642 2003.
643 Lebo, Z.: A Numerical Investigation of the Potential Effects of Aerosol-Induced Warming and
644 Updraft Width and Slope on Updraft Intensity in Deep Convective Clouds, J Atmos Sci,
645 75, 535-554, doi: 10.1175/Jas-D-16-0368.1, 2018.
646 Lebo, Z. J., and Seinfeld, J. H.: Theoretical basis for convective invigoration due to increased
647 aerosol concentration, Atmos Chem Phys, 11, 5407-5429, doi: 10.5194/acp-11-5407-2011,
648 2011.
649 Lebo, Z. J., Morrison, H., and Seinfeld, J. H.: Are simulated aerosol-induced effects on deep
650 convective clouds strongly dependent on saturation adjustment? Atmos Chem Phys, 12,
651 9941-9964, doi: 10.5194/acp-12-9941-2012, 2012.
652 Lee, S. S., Li, Z. Q., Zhang, Y. W., Yoo, H., Kim, S., Kim, B. G., Choi, Y. S., Mok, J., Um, J.,
653 Choi, K. O., and Dong, D. H.: Effects of model resolution and parameterizations on the
654 simulations of clouds, precipitation, and their interactions with aerosols, Atmos Chem Phys,
655 18, 13-29, doi: 10.5194/acp-18-13-2018, 2018.

656 Li, G. H., Wang, Y., and Zhang, R. Y.: Implementation of a two-moment bulk microphysics
657 scheme to the WRF model to investigate aerosol-cloud interaction, J Geophys Res-Atmos,
658 113, D15211, doi: 10.1029/2007jd009361, 2008.
659 Li, X. W., Tao, W. K., Khain, A. P., Simpson, J., and Johnson, D. E.: Sensitivity of a Cloud-
660 Resolving Model to Bulk and Explicit Bin Microphysical Schemes. Part I: Comparisons, J
661 Atmos Sci, 66, 3-21, doi: 10.1175/2008jas2646.1, 2009.
662 Li, Z. Q., Niu, F., Fan, J. W., Liu, Y. G., Rosenfeld, D., and Ding, Y. N.: Long-term impacts of
663 aerosols on the vertical development of clouds and precipitation, Nat Geosci, 4, 888-894,
664 doi: 10.1038/Ngeo1313, 2011.
665 Loftus, A. M., and Cotton, W. R.: Examination of CCN impacts on hail in a simulated supercell
666 storm with triple-moment hail bulk microphysics, Atmos Res, 147, 183-204, doi:
667 10.1016/j.atmosres.2014.04.017, 2014.
668 Lohmann, U., and Feichter, J.: Global indirect aerosol effects: a review, Atmos Chem Phys, 5,
669 715-737, doi: 10.5194/acp-5-715-2005, 2005.
670 Milbrandt, J. A., and Yau, M. K.: A multimoment bulk microphysics parameterization. Part II: A
671 proposed three-moment closure and scheme description, J Atmos Sci, 62, 3065-3081, doi:
672 10.1175/Jas3535.1, 2005.
673 Morrison, H., Curry, J. A., and Khvorostyanov, V. I.: A new double-moment microphysics
674 parameterization for application in cloud and climate models. Part I: Description, J Atmos
675 Sci, 62, 1665-1677, doi: 10.1175/Jas3446.1, 2005.
676 Morrison, H., and W. W.Grabowski: Comparison of bulk and bin warm-rain microphysics models
677 using a kinematic framework.J. Atmos. Sci., 64, 2839–2861, 2007.

678 Morrison, H., and W. W. Grabowski: Modeling supersaturation and subgrid-scale mixing with
679 two-moment bulk warm microphysics, J. Atmos. Sci., 65, 792–812,
680 doi:10.1175/2007JAS2374.1, 2008.
681 Morrison, H., Thompson, G., and Tatarskii, V.: Impact of Cloud Microphysics on the Development
682 of Trailing Stratiform Precipitation in a Simulated Squall Line: Comparison of One- and
683 Two-Moment Schemes, Mon Weather Rev, 137, 991-1007, doi: 10.1175/2008mwr2556.1,
684 2009.
685 Morrison, H., and Milbrandt, J.: Comparison of Two-Moment Bulk Microphysics Schemes in
686 Idealized Supercell Thunderstorm Simulations, Mon Weather Rev, 139, 1103-1130, doi:
687 10.1175/2010mwr3433.1, 2011.
688 Morrison, H.: On the robustness of aerosol effects on an idealized supercell storm simulated with
689 a cloud system-resolving model, Atmos Chem Phys, 12, 7689-7705, doi: 10.5194/acp-12-
690 7689-2012, 2012.
691 Pinsky M., I.P. Mazin, A. Korolev, and A.P. Khain: Supersaturation and diffusional droplet growth
692 in liquid clouds. J. Atmos. Sci. 70, 2778-2793, 2013.
693 Politovich, M. K., and W. A. Cooper: Variability of the supersaturation in cumulus clouds. J.
694 Atmos. Sci., 45, 1651–1664, doi:10.1175/1520-0469(1988)045,1651:VOTSIC.2.0.CO;2,
695 1988.
696 Rosenfeld, D., Lohmann, U., Raga, G. B., O'Dowd, C. D., Kulmala, M., Fuzzi, S., Reissell, A.,
697 and Andreae, M. O.: Flood or drought: How do aerosols affect precipitation?, Science, 321,
698 1309-1313, doi: 10.1126/science.1160606, 2008.
699 Rosenfeld, D., Andreae, M. O., Asmi, A., Chin, M., de Leeuw, G., Donovan, D. P., Kahn, R.,
700 Kinne, S., Kivekas, N., Kulmala, M., Lau, W., Schmidt, K. S., Suni, T., Wagner, T., Wild,

M., and Quaas, J.: Global observations of aerosol-cloud-precipitation-climate interactions, Rev Geophys, 52, 750-808, doi: 10.1002/2013rg000441, 2014.

Rosenfeld, D., Zheng, Y. T., Hashimshoni, E., Pohlker, M. L., Jefferson, A., Pohlker, C., Yu, X., Zhu, Y. N., Liu, G. H., Yue, Z. G., Fischman, B., Li, Z. Q., Giguzin, D., Goren, T., Artaxo, P., Barbosa, H. M. J., Poschl, U., and Andreae, M. O.: Satellite retrieval of cloud condensation nuclei concentrations by using clouds as CCN chambers, P Natl Acad Sci USA, 113, 5828-5834, doi: 10.1073/pnas.1514044113, 2016.

Salamanca, F., and Martilli, A.: A new Building Energy Model coupled with an Urban Canopy Parameterization for urban climate simulations-part II. Validation with one dimension off-line simulations, Theor Appl Climatol, 99, 345-356, doi: 10.1007/s00704-009-0143-8, 2010.

Sheffield, A. M., Saleeby, S. M., and van den Heever, S. C.: Aerosol-induced mechanisms for cumulus congestus growth, J Geophys Res-Atmos, 120, 8941-8952, doi: 10.1002/2015jd023743, 2015.

Skamarock, W. C., Klemp, J. B., Dudhia, J., Gill, D. O., Barker, D. M., Duda, M., Huang, X. Y., Wang, W., and Powers, J. G.: A description of the advanced research WRF version 3, NCAR, Tech. Note, Mesoscale and Microscale Meteorology Division, National Center for Atmospheric Research, Boulder, Colorado, USA, 2008.

Stevens, B., and G.Feingold: Untangling aerosol effects on clouds and precipitation in a buffered system. Nature, 461, 607–613, 2009.

Storer, R. L., van den Heever, S. C., and Stephens, G. L.: Modeling Aerosol Impacts on Convective Storms in Different Environments, J Atmos Sci, 67, 3904-3915, doi: 10.1175/2010jas3363.1, 2010.

724 Tao, W., and X. Li: The relationship between latent heating, vertical velocity, and precipitation
725 processes: The impact of aerosols on precipitation in organized deep convective systems,
726 J. Geophys. Res. Atmos., 121(11), 6299-6320, 2016.
727 Varble A.: Erroneous attribution of deep convective invigoration to aerosol concentration. J Atmos
728 Sci, 75(4):1351–68, 2018.
729 van den Heever, S. C., G. L.Stephens, and N. B.Wood: Aerosol indirect effects on tropical
730 convection characteristics under conditions of radiative-convective equilibrium. J. Atmos.
731 Sci., 68, 699–718, 2011.
732 Wang, Y., Fan, J. W., Zhang, R. Y., Leung, L. R., and Franklin, C.: Improving bulk microphysics
733 parameterizations in simulations of aerosol effects, J Geophys Res-Atmos, 118, 5361-5379,
734 doi: 10.1002/jgrd.50432, 2013.
735 Wiedinmyer, C., Akagi, S. K., Yokelson, R. J., Emmons, L. K., Al-Saadi, J. A., Orlando, J. J., and
736 Soja, A. J.: The Fire INventory from NCAR (FINN): a high resolution global model to
737 estimate the emissions from open burning, Geosci Model Dev, 4, 625-641, doi:
738 10.5194/gmd-4-625-2011, 2011.
739 Yuan, T. L., Li, Z. Q., Zhang, R. Y., and Fan, J. W.: Increase of cloud droplet size with aerosol
740 optical depth: An observation and modeling study, J Geophys Res-Atmos, 113, D04201,
741 doi: 10.1029/2007jd008632, 2008.
742 Zaveri, R. A., Easter, R. C., Fast, J. D., and Peters, L. K.: Model for Simulating Aerosol
743 Interactions and Chemistry (MOSAIC), J Geophys Res-Atmos, 113, D13204, doi:
744 10.1029/2007jd008782, 2008.
745

746 **Table 1** Descriptions of the PM2.5 Monitoring Sites over the Houston area from TCEQ

Abbreviation	Site Descriptions	Latitude	Longitude
HA	Houston Aldine	29.901	-95.326
HDP	Houston Deer Park 2	29.670	-95.129
SFP	Seabrook Friendship Park	29.583	-95.016
CR	Conroe Relocated	30.350	-95.425
KW	Kingwood	30.058	-95.190
CT	Clinton	29.734	-95.258
PP	Park Place	29.686	-95.294
GS	Galveston 99th Street	29.254	-94.861

747

748

749

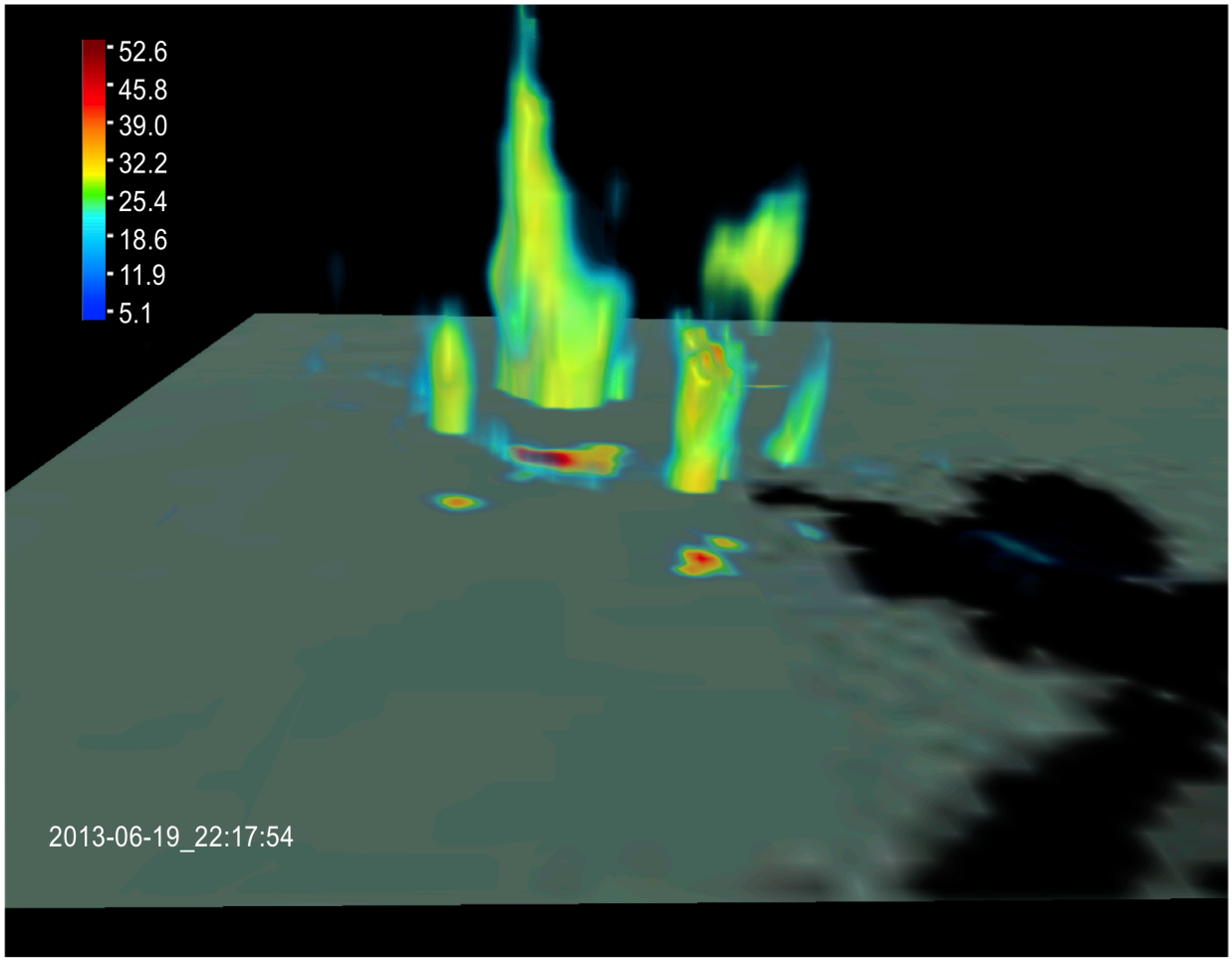

Figure 1 3D structure snapshot of radar reflectivity (unit: dBZ) from NEXRAD, overlaid with the composite reflectivity shown on the surface at the time when the maximum reflectivity is observed (2217 UTC). The dark shade shows the water body and the largest cell is in the Houston.

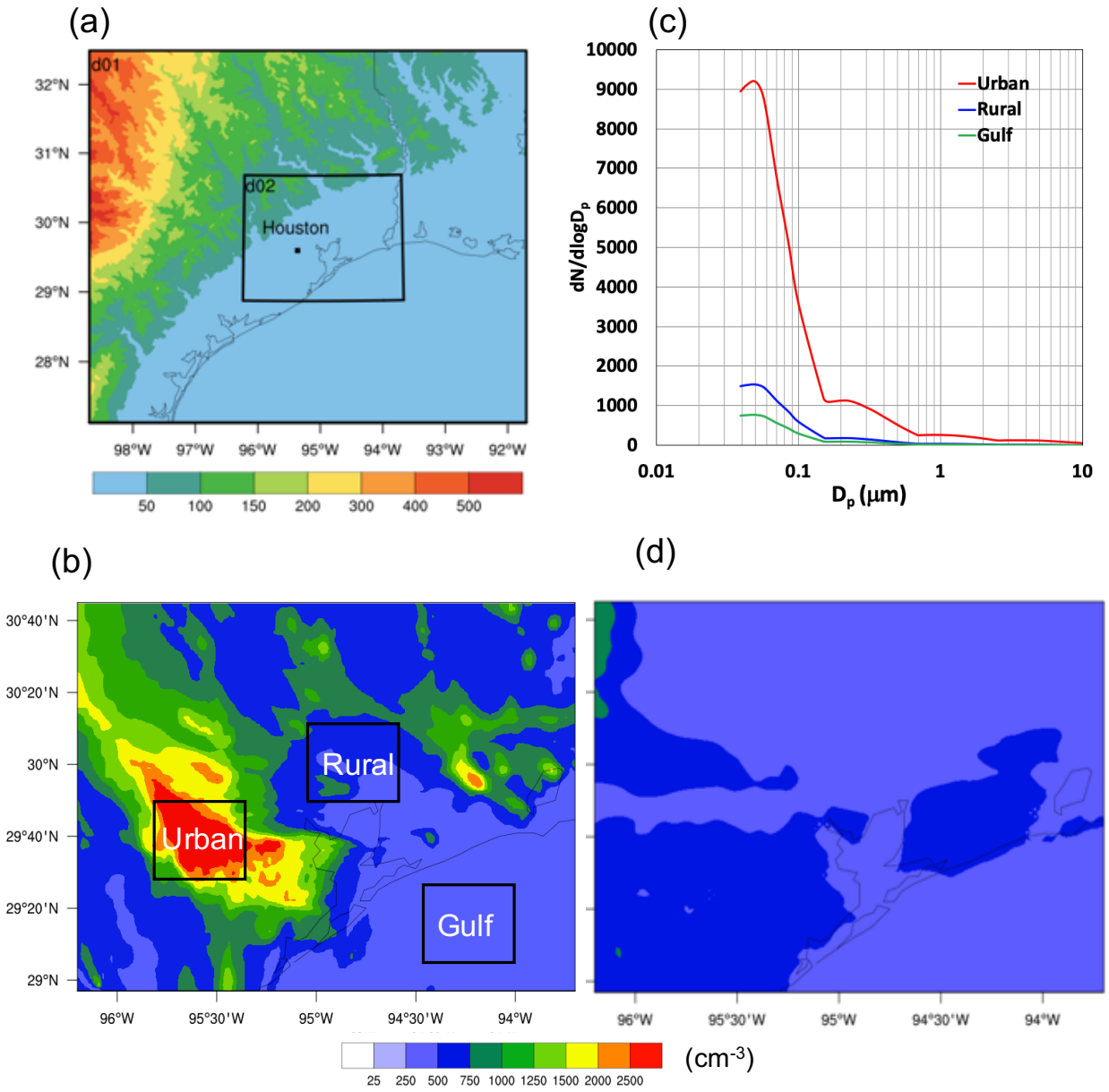

Figure 2 (a) Simulation domains with the terrain heights (unit: m), (b) aerosol number concentration (unit: cm^{-3}) from D1_MOR_anth, (c) aerosol size distributions over the urban, rural, and Gulf of Mexico as marked by three black boxes in Fig. 2b at 1200 UTC, 19 Jun 2013 (6-hr before the convection initiation), and (d) the same as Fig. 2b, but for D1_MOR_noanth in which the anthropogenic aerosols are excluded.

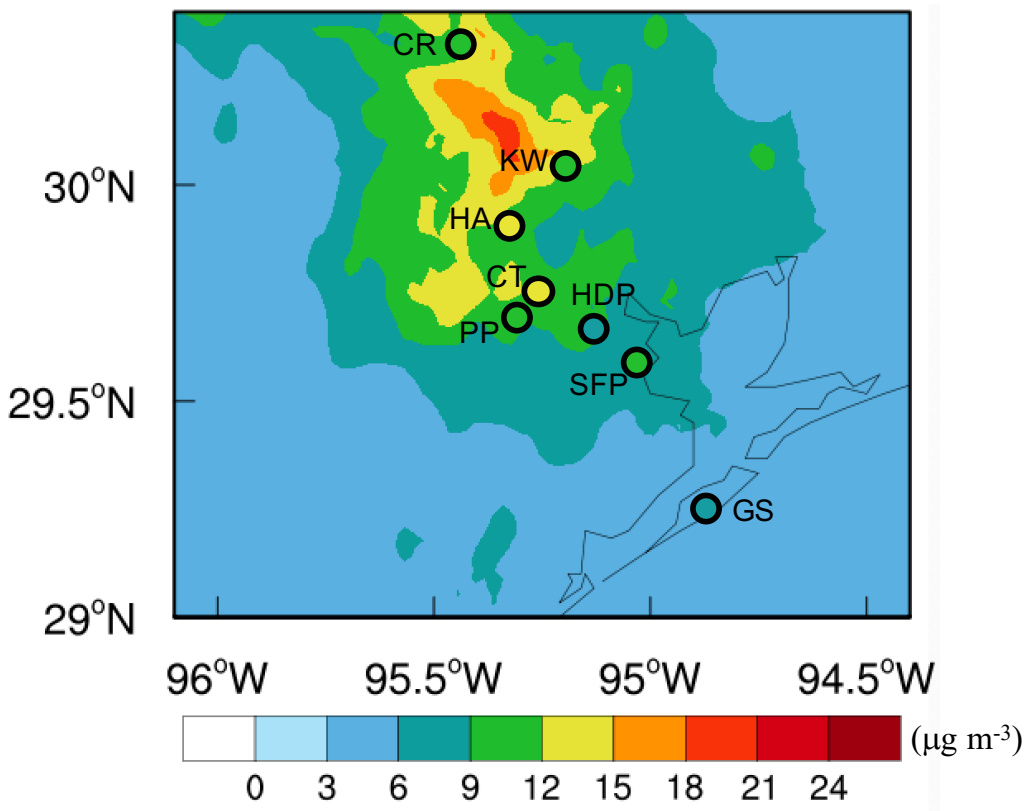

762

763 **Figure 3** Comparisons of 24-hr averaged PM2.5 mass concentrations (unit: μg m^{-3}) between model
764 simulation D1_MOR_anth (contoured) and site observation from TCEQ (colored circles) from
765 1800 UTC, 18 June 2013 to 1800 UTC, 19 June 2013 (1 day before the convection initiation). The
766 site names and other information are shown in Table 1.

767

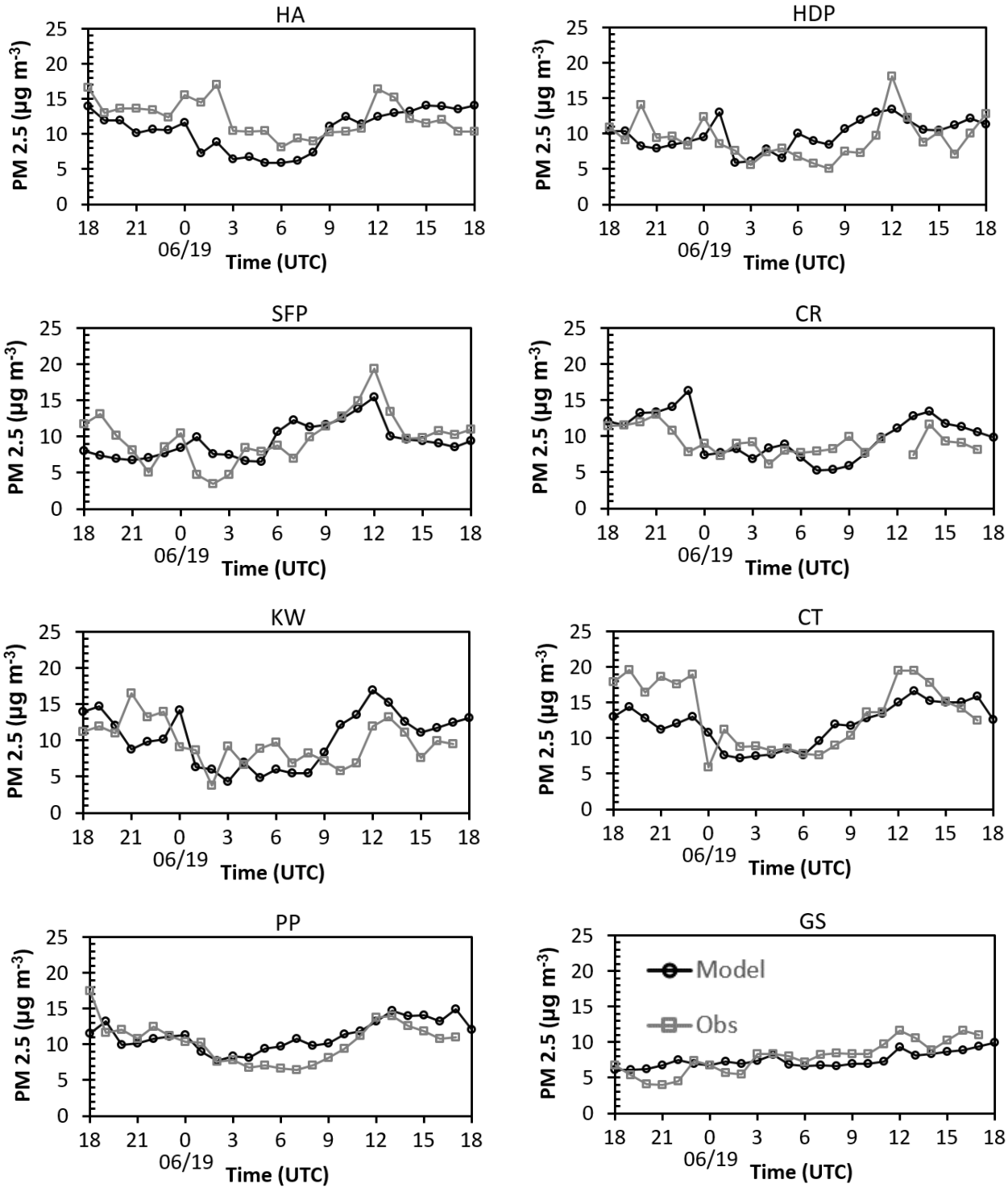

Figure 4 Site-by-site comparisons of hourly PM2.5 mass concentrations (unit: µg m^{-3}) from D1_MOR_anth and TCEQ site observation over 24 hours from 1800 UTC, 18 June 2013 to 1800 UTC, 19 June 2013 (1 day before the convection initiation).

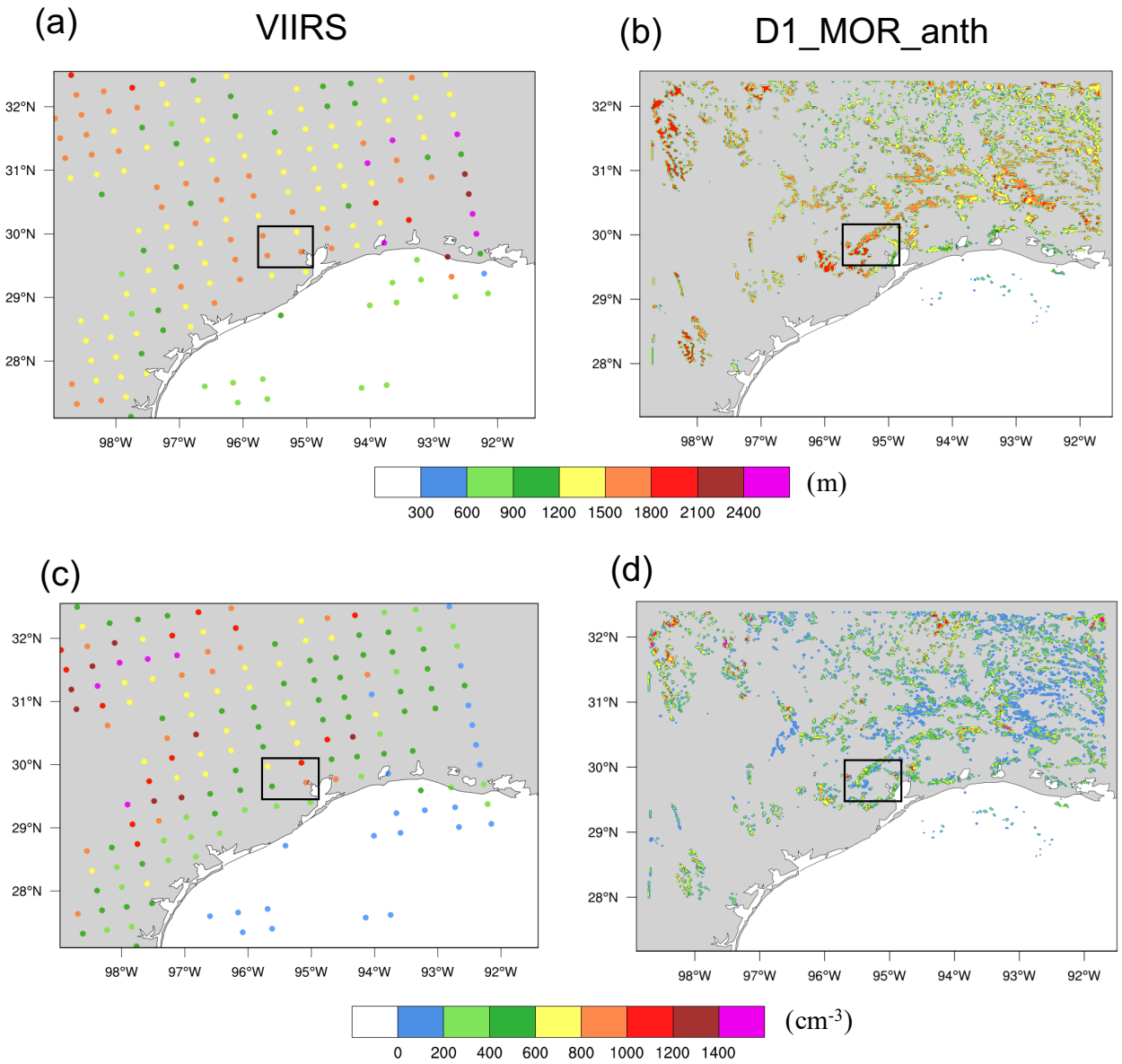

772

773 **Figure 5** Evaluation of (a,b) cloud base heights (unit: m) and (c,d) CCN number concentration at
774 cloud base (unit: cm^{-3}) from VIIRS satellite (left) retrieved at 1943 UTC (Rosenfeld et al. 2016)
775 and model simulation D1_MOR_anth (right) at 2000 UTC, 19 June 2013. The Houston area is
776 marked as the black box. Satellite-retrieved cloud base height was calculated from the difference
777 between reanalysis surface air temperature (from reanalysis data) and VIIRS-measured cloud base
778 temperature (warmest cloudy pixel) divided by the dry adiabatic lapse rate, while modeled cloud
779 base height was determined by the lowest cloud layer with cloud mass mixing ratio greater than
780 10^{-5} kg kg^{-1}.

781

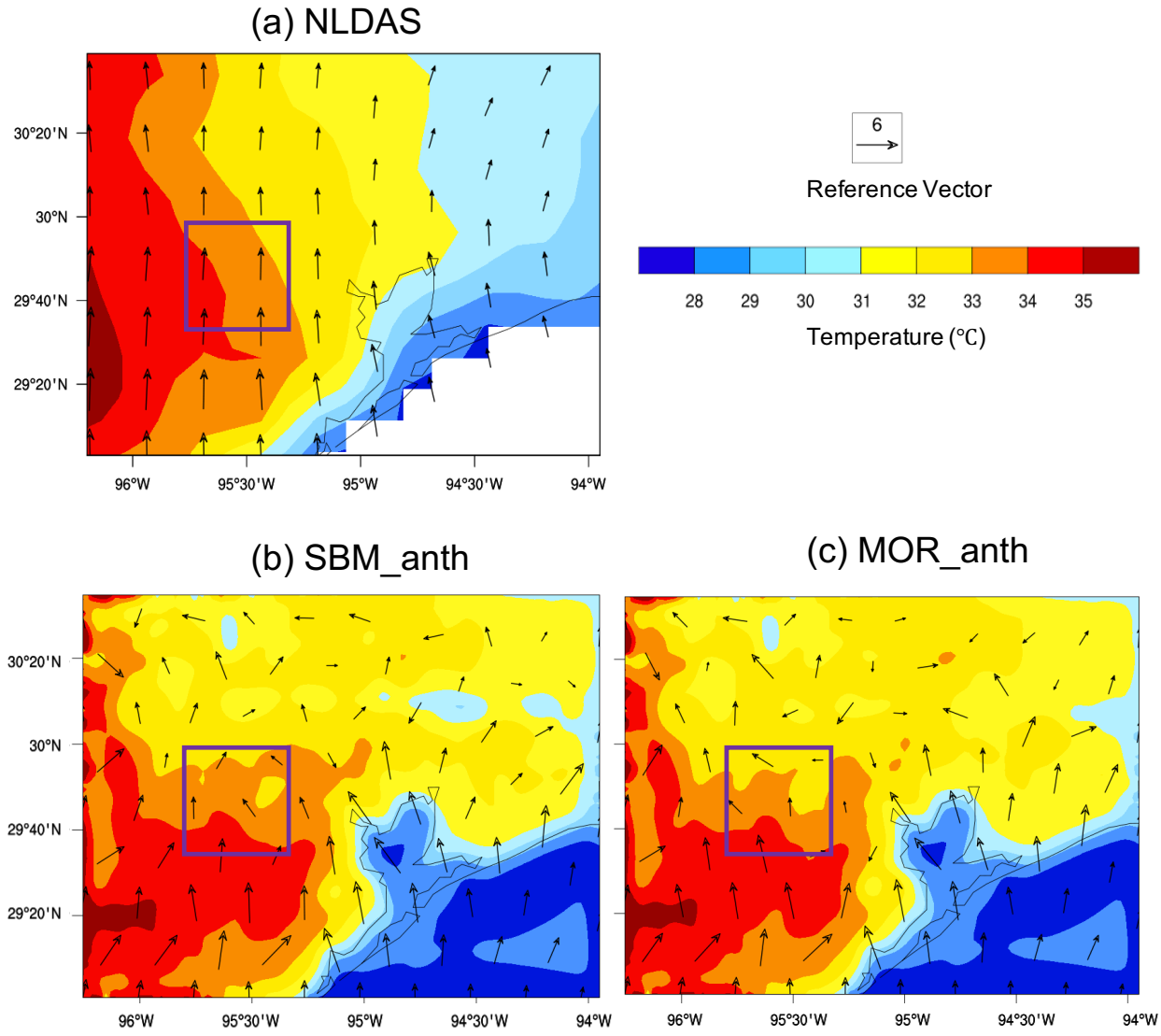

782

783 **Figure 6** 2-m Temperature (shaded; unit: ℃) and 10-m winds (vectors; unit: m s^{-1}) from (a)
784 NLDAS, (b) SBM_anth and (c) MOR_anth at 1800 UTC, 19 Jun 2013. The purple box denotes
785 the Houston area.

786

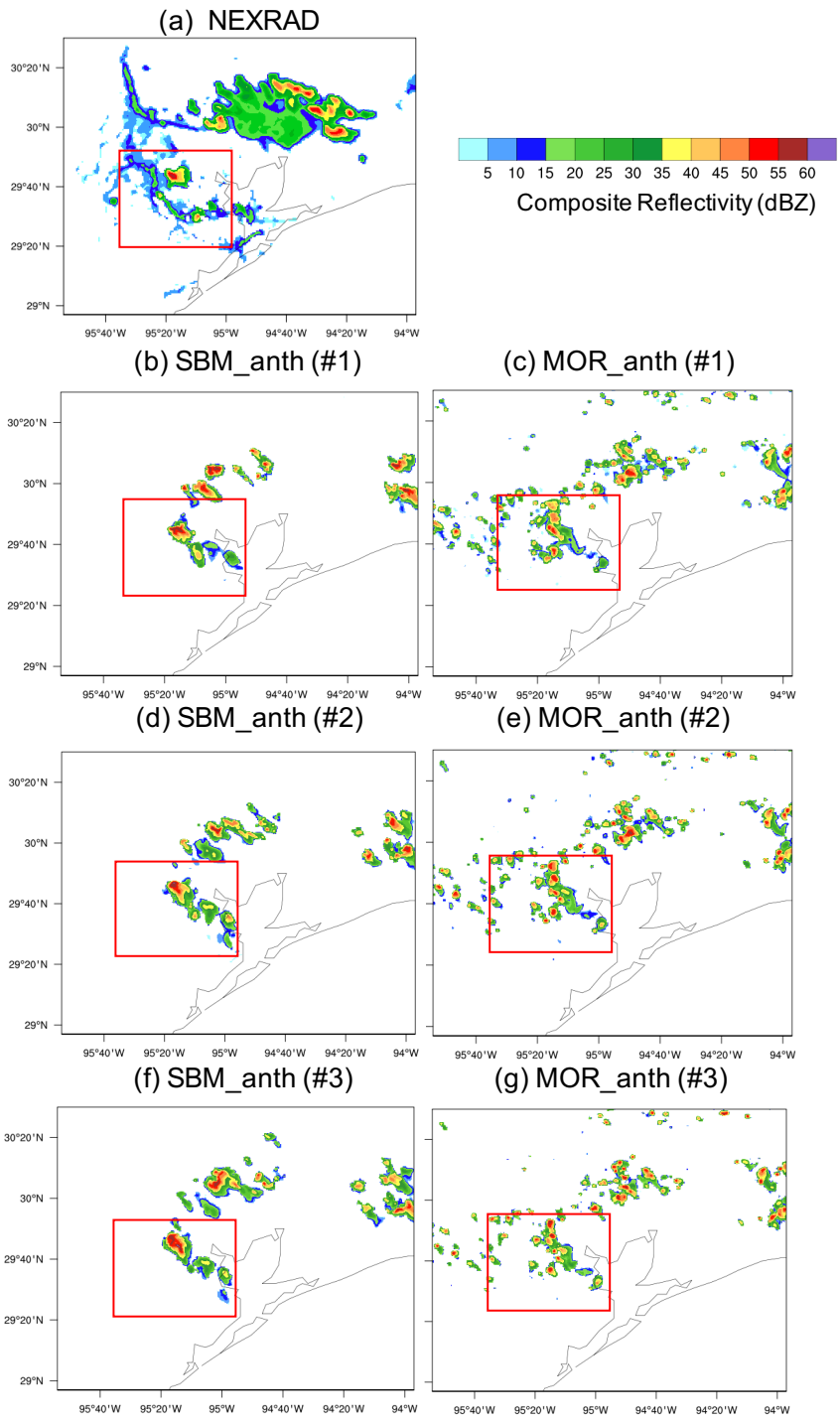

787

788 **Figure 7** Composite reflectivity (unit: dBZ) from (a) NEXRAD (2217 UTC), (b, d, f) three
789 ensemble runs for SBM_anth (2140 UTC) and (c, e, g) three ensemble runs for MOR_anth (2125
790 UTC) when maximum reflectivity in Houston is observed on 19 June 2013. The red box is the
791 study area for convection cells near Houston.

792

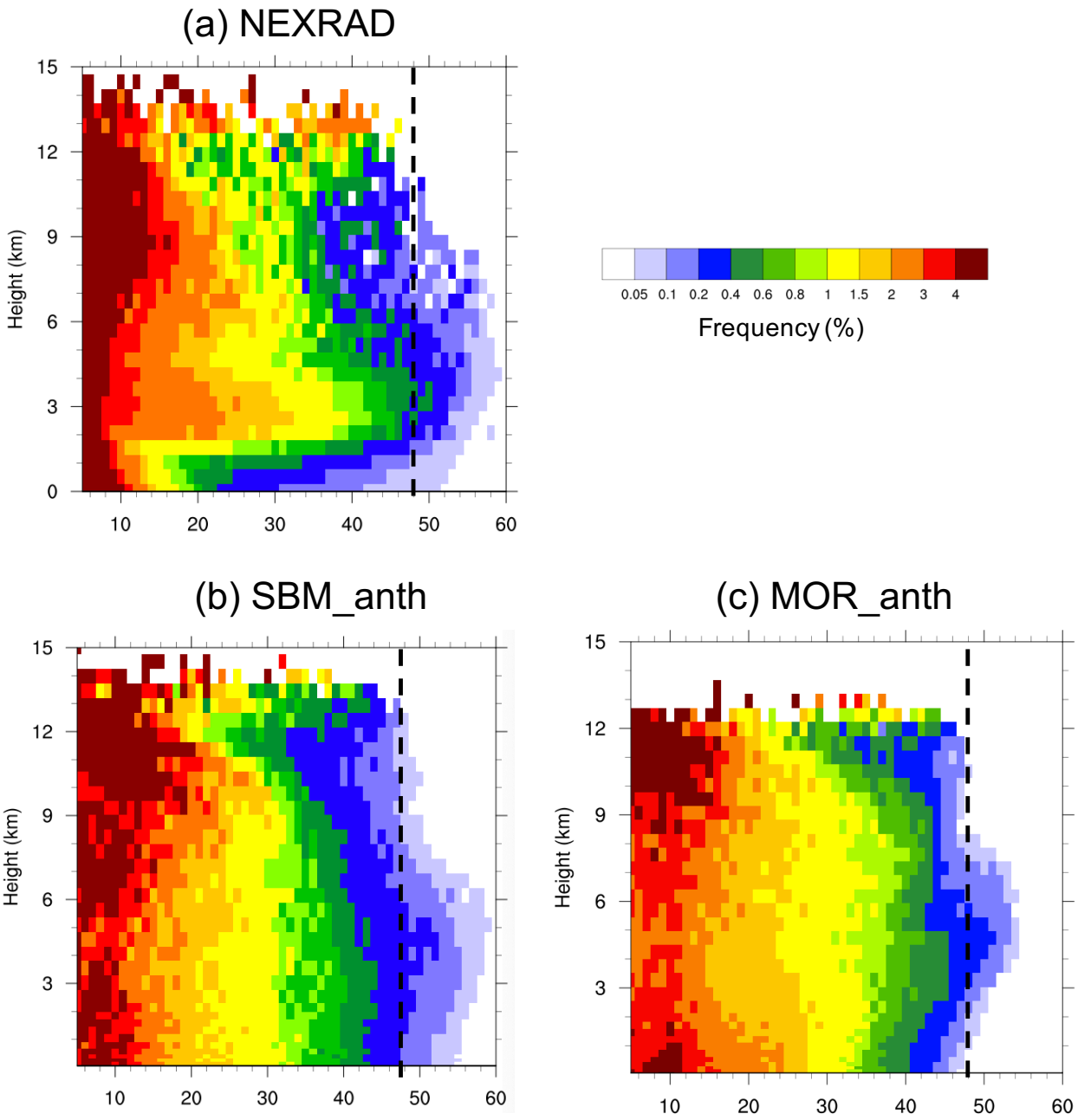

Figure 8 The CFAD of reflectivity (unit: dBZ) for the values larger than 0 dBZ from (a) NEXRAD, (b) SBM_anth and (c) MOR_anth over the study area (red box in Fig. 7) from 1800 UTC, 19 Jun to 0000 UTC, 20 Jun 2013. The black solid lines denote the reflectivity with the value of 48 dBZ. The results are the three ensemble means.

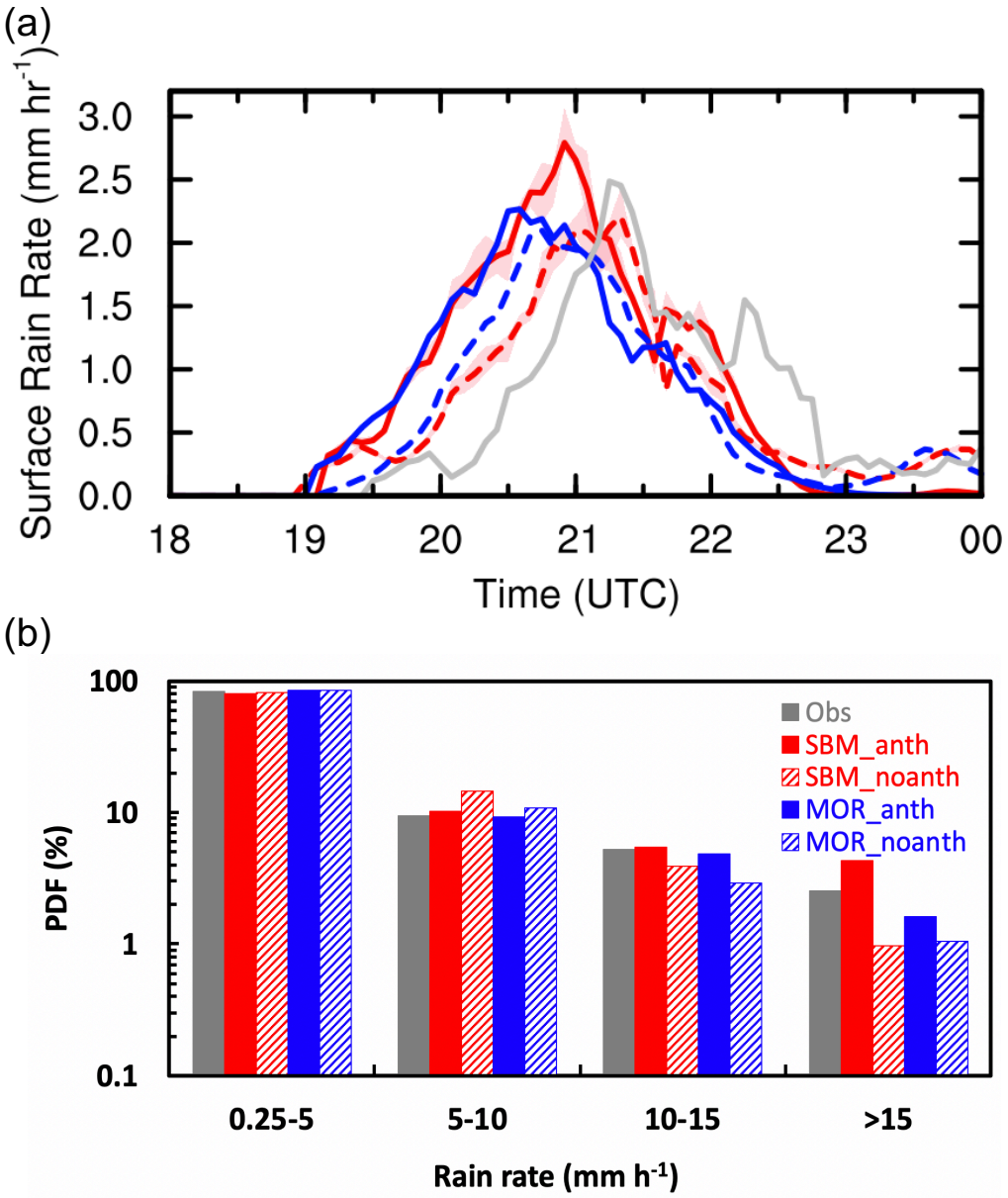

Figure 9 (a) Time series of averaged surface rain rate (unit: mm h^{-1}) and (b) PDFs of rain rate for the values larger than 0.25 mm h^{-1} over the study area (red box in Fig. 7) from observation (grey), SBM_anth and SBM_noanth (red), MOR_anth and MOR_noanth (blue) from 1800UTC, 19 Jun 2013 to 0000 UTC, 20 Jun 2013. The observed precipitation rate is obtained by NEXRAD retrieved rain rate. Both observation and model data are in every 5-min frequency. The results are the three ensemble means. The shaded areas mark the spread of the ensemble members.

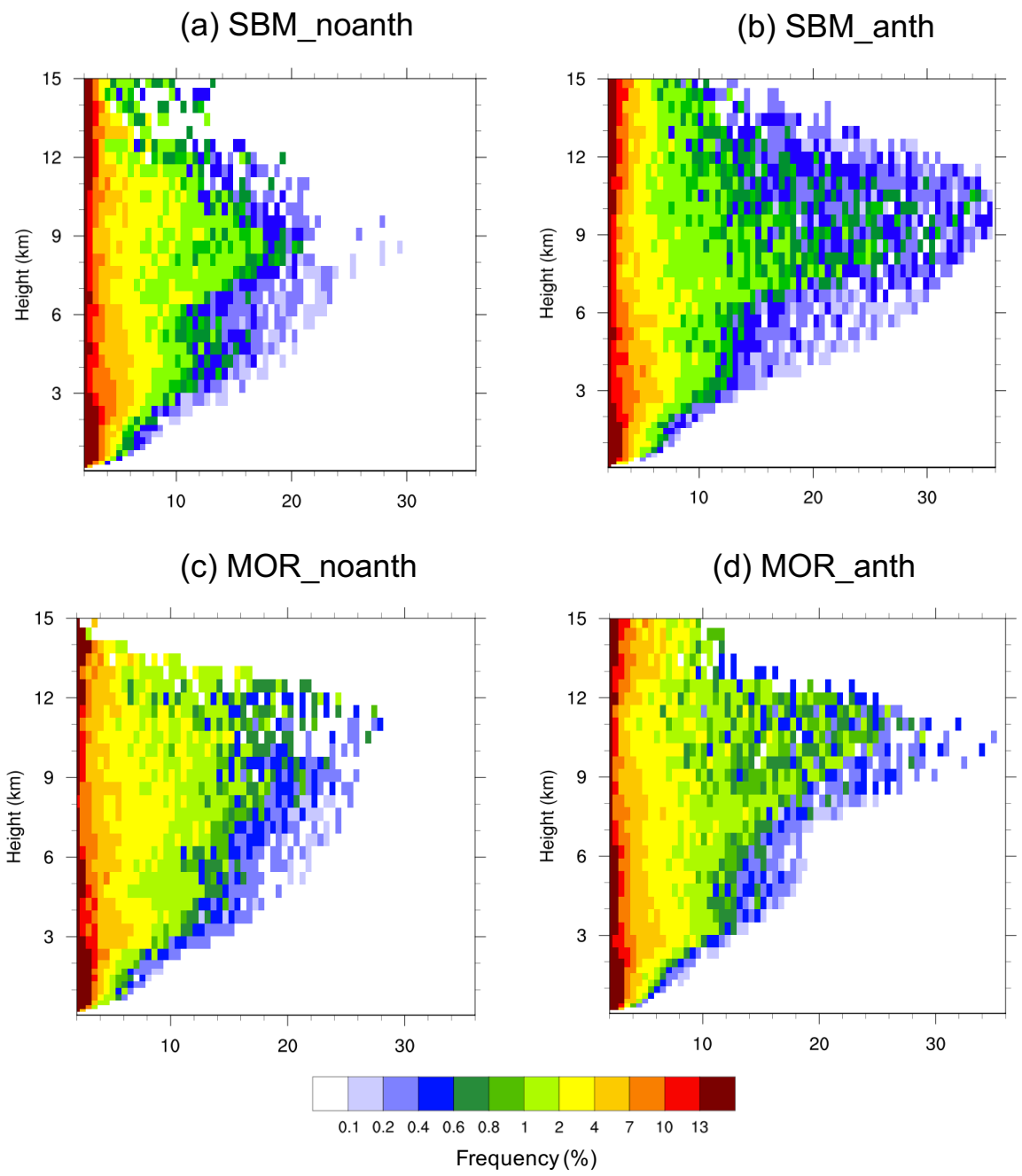

809

810 **Figure 10** CFADs of updraft velocity (unit: m s^{-1}) for values larger than 2 m s^{-1} from (a)
811 SBM_noanth, (b) SBM_anth, (c) MOR_noanth, and (d) MOR_anth over the study area (red box
812 in Fig. 7) during the strong convection period (2000 – 2300 UTC, 19 Jun 2013). The results are
813 the three ensemble means.

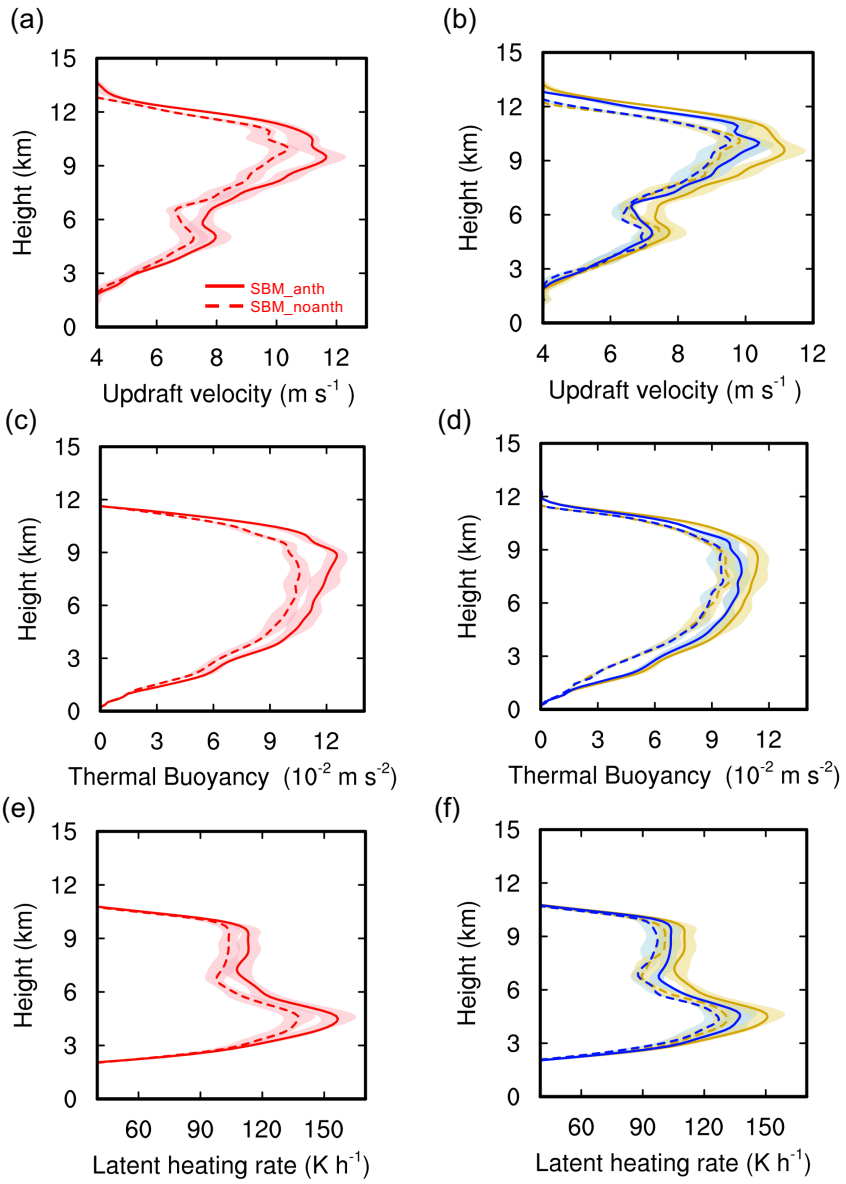

Figure 11 Vertical profiles of (a,b) updraft velocity (unit: m s^{-1}) , (c,d) thermal buoyancy (unit: m s^{-2}) and (e,f) total latent heating rate (unit: K h^{-1}) averaged over the top 25 percentiles (i.e., from 75th to 100th) of the updrafts with velocity greater than 2 m s^{-1} from the simulations SBM_anth and SBM_noanth (red), MOR_anth and MOR_noanth (blue), and MOR_SS_anth and MOR_SS_noanth (orange) over the study area (red box in Fig. 7) during the strong convection period (2000 – 2300 UTC, 19 Jun 2013). The results are the three ensemble means. The shaded areas mark the spread of the ensemble members.

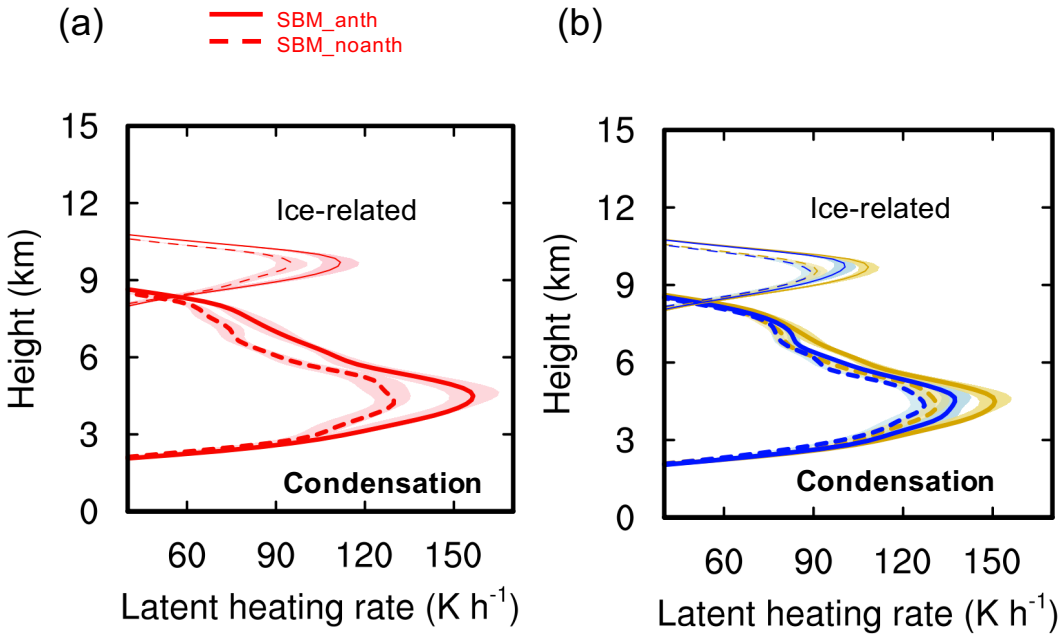

Figure 12 Vertical profiles of condensation heating rate (thick lines below 9 km; unit: K h^{-1}) and ice-related latent heating rate (thin lines above 9 km; unit: K h^{-1}) averaged over the top 25 percentiles (i.e., 75th to 100th) of the updrafts with velocity greater than 2 m s^{-1} from the simulations (a) SBM_anth and SBM_noanth (red), and (b) MOR_anth and MOR_noanth (blue), and MOR_SS_anth and MOR_SS_noanth (orange) over the study area (red box in Fig. 7) during the strong convection period (2000 – 2300 UTC, 19 Jun 2013). Data are processed in the same way as Figure 11.

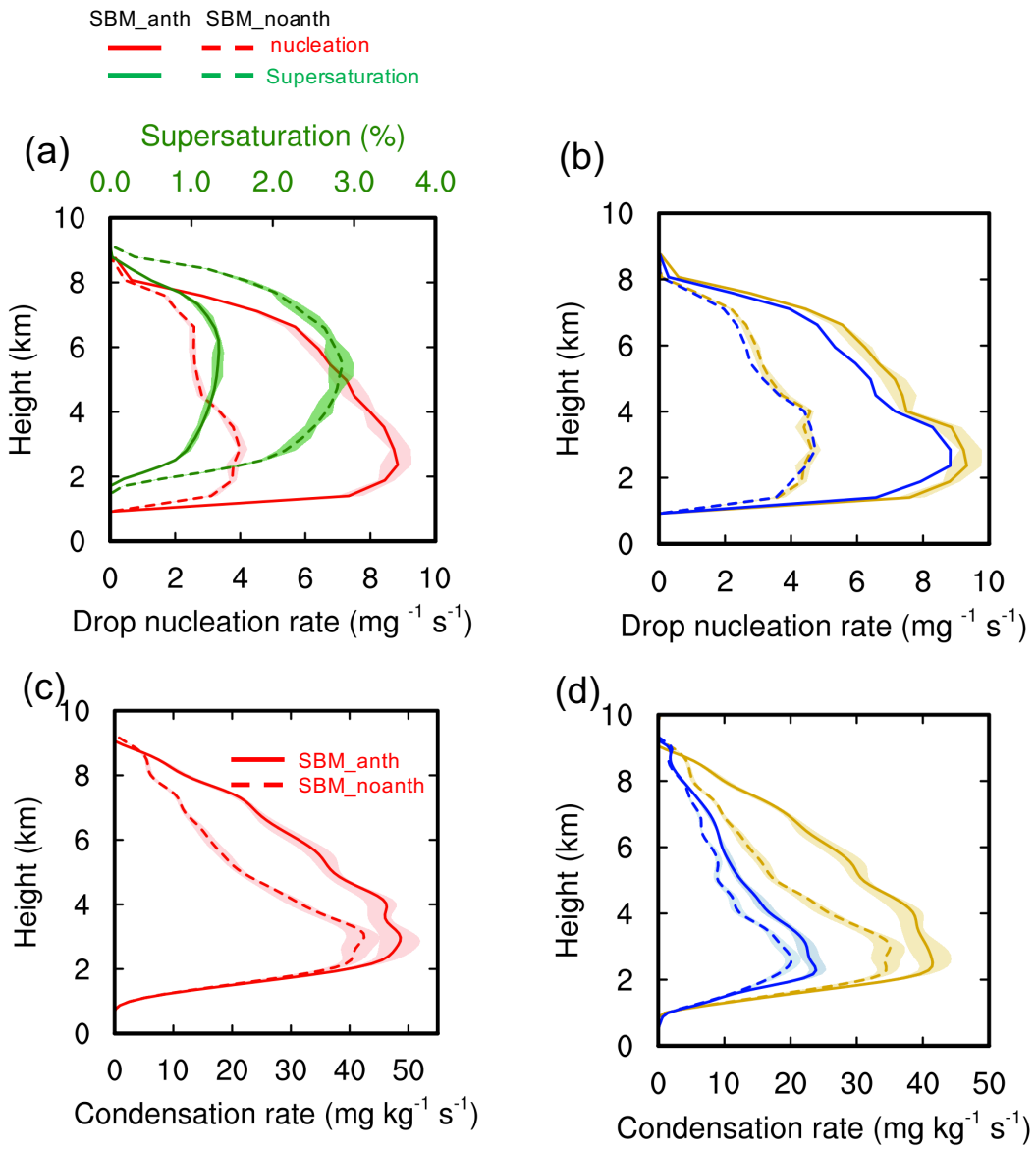

Figure 13 Vertical profiles of (a) drop nucleation rate (red; unit: mg^{-1} s^{-1}) and supersaturation with respect to water (green; unit: %) from SBM_anth and SBM_noanth, (b) drop nucleation rate (unit: mg^{-1} s^{-1}) from MOR_anth and MOR_noanth (blue), and MOR_SS_anth and MOR_SS_noanth (orange), (c) condensation rate (unit: mg kg^{-1} s^{-1}) from SBM_anth and SBM_noanth (red), and (d) the same as (c) but from MOR_anth and MOR_noanth (blue), and MOR_SS_anth and MOR_SS_noanth (orange), averaged over the top 25 percentiles (i.e., from 75th to 100th) of the updrafts with velocity greater than 2 m s^{-1} over the study area (red box in Fig. 7) during the strong convection period (2000 – 2300 UTC, 19 Jun 2013). Data are processed in the same way as Figure 11.

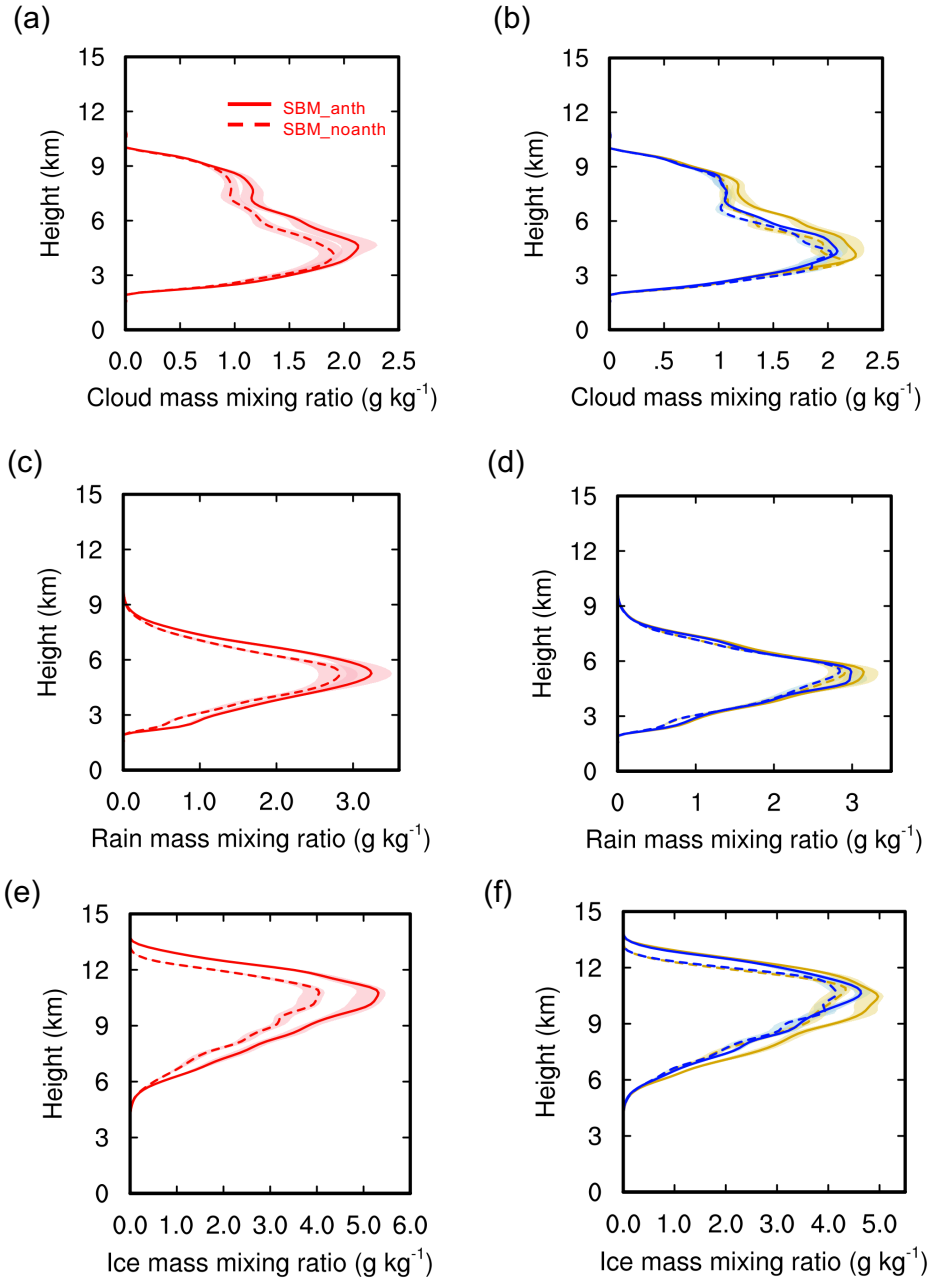

842

843 **Figure 14** Vertical profiles of (a, b) cloud droplet, (c, d) rain drop and (e, f) ice particle (including
844 ice, snow, and graupel) mass mixing ratios (unit: g kg^{-1}) averaged over the top 25 percentiles (i.e.,
845 75th to 100th) of the updrafts with value greater than 2 m s^{-1} from the simulations SBM_anth and
846 SBM_noanth (red), MOR_anth and MOR_noanth (blue), and MOR_SS_anth and
847 MOR_SS_noanth (orange) over the study area (red box in Fig. 7) during the strong convection
848 period (2000 – 2300 UTC, 19 Jun 2013). Data are processed in the same way as Figure 11.

849

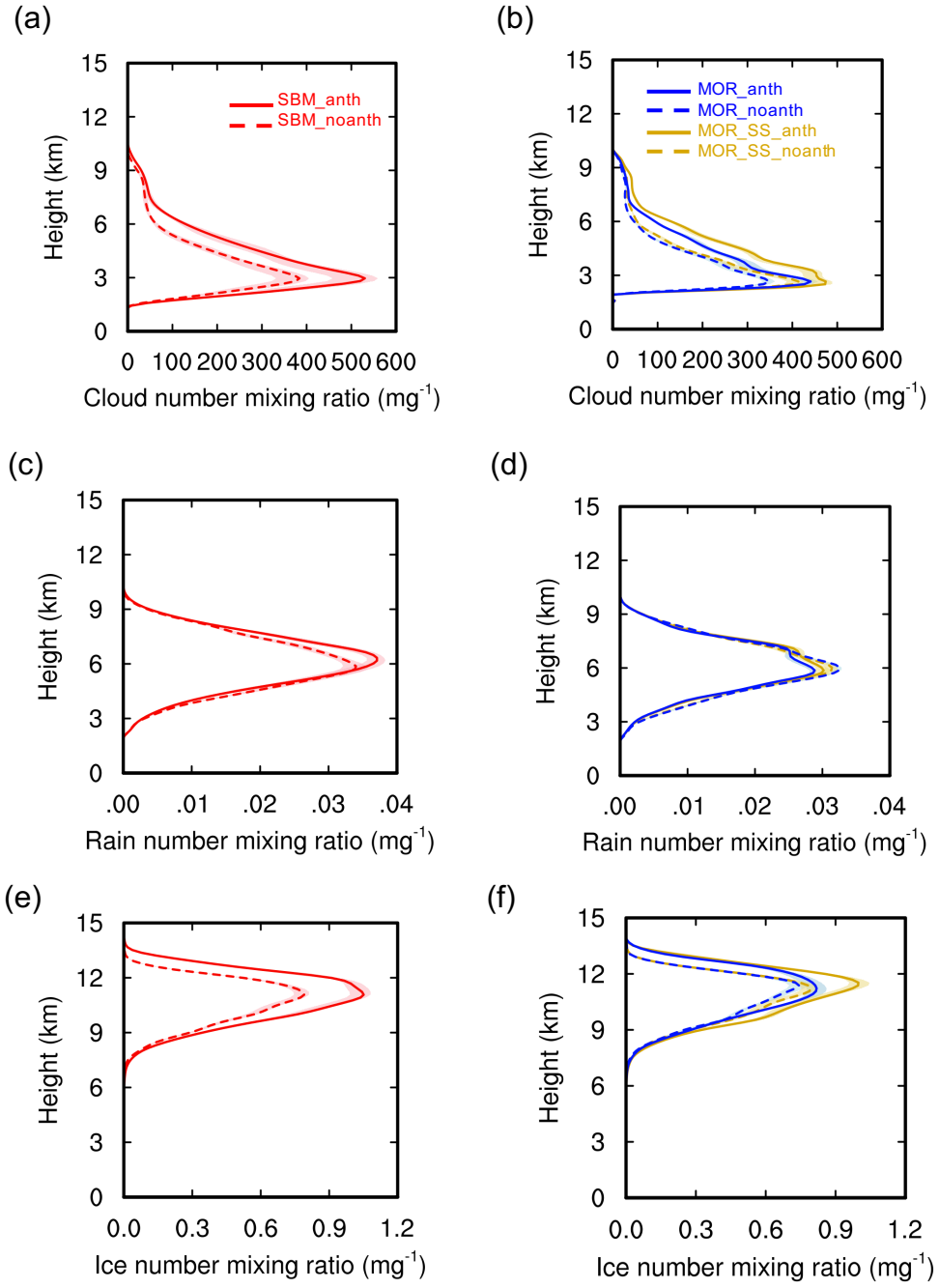

850

851 **Figure 15** Same as Figure 14, but for hydrometeor number mixing ratio.

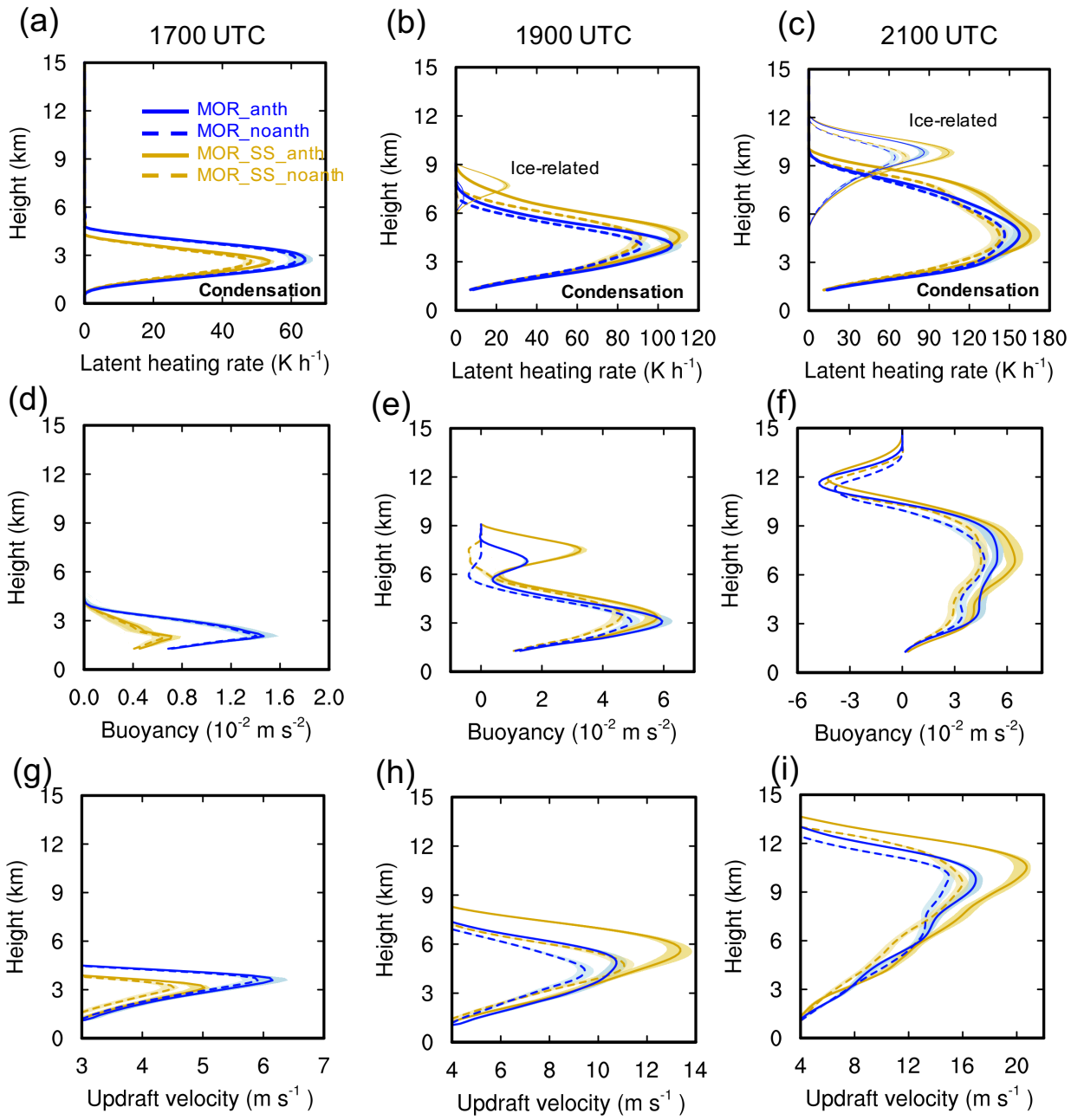

Figure 16 Vertical profiles of (a-c) latent heating rate from condensation (weighted lines) and ice-related processes (freezing, riming, and deposition; thin lines), (d-f) total buoyancy, (g-i) updraft velocity averaged over the top 25 percentiles (i.e., 75th to 100th) of the updrafts with value greater than 2 ms^{-1} from the simulations MOR_anth, MOR_noanth, MOR_SS_anth, and MOR_SS_noanth over the analysis domain as shown in the red box in Figure 7 at 1700 UTC, 1900 UTC and 2100 UTC. Data are processed in the same way as Figure 11.

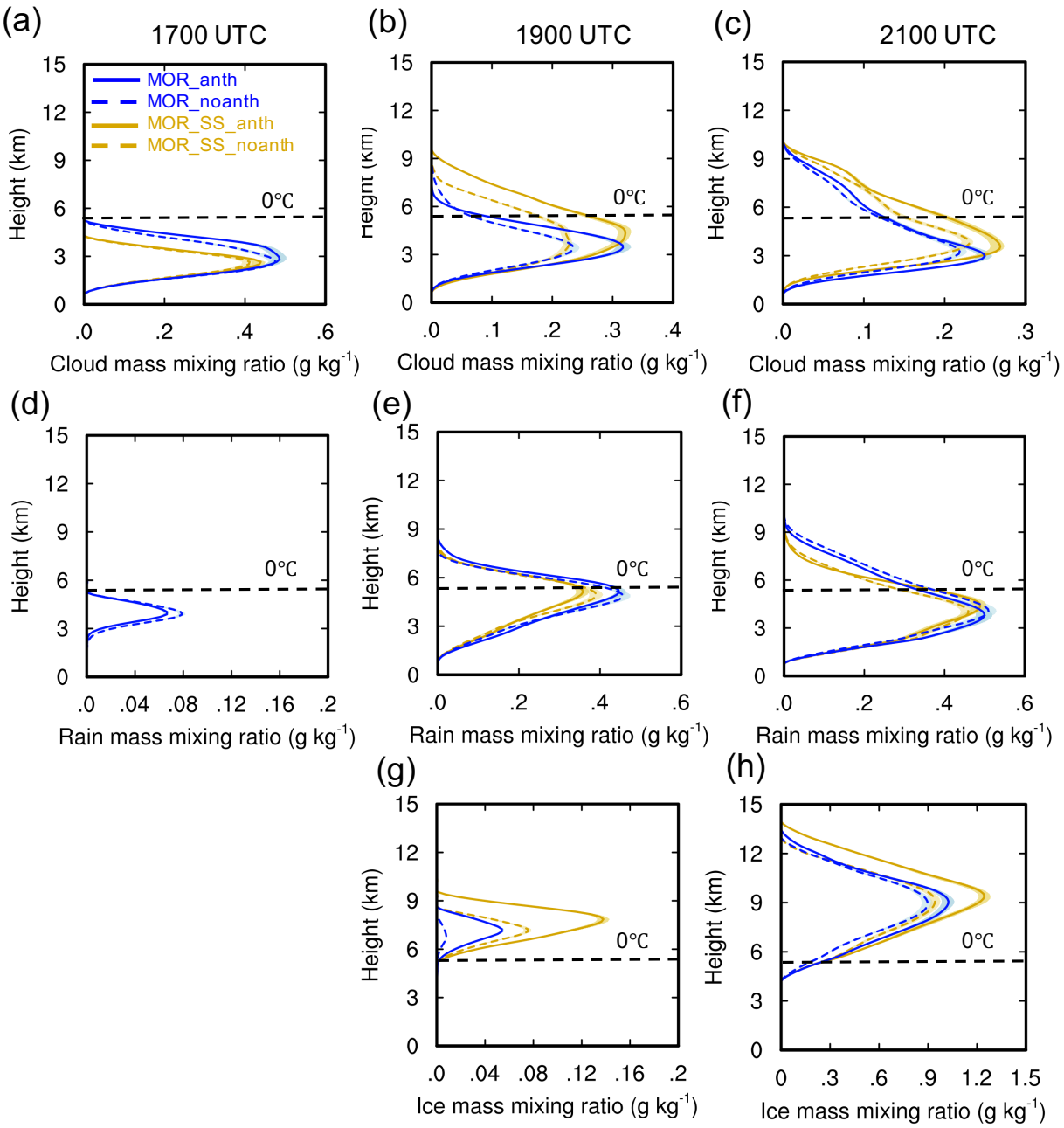

Figure 17 Vertical profiles mass mixing ratios of (a-c) cloud droplet, (d-f) rain drop and (g-h) ice particle (including ice, snow, and graupel) averaged over cloudy points (hydrometeor mass larger than 10^{-5} kg kg^{-1}) from the simulations MOR_anth, MOR_noanth, MOR_SS_anth, and MOR_SS_noanth over the analysis domain as shown in the red box in Figure 7 at 1700 UTC, 1900 UTC and 2100 UTC. Data are processed in the same way as Figure 11.

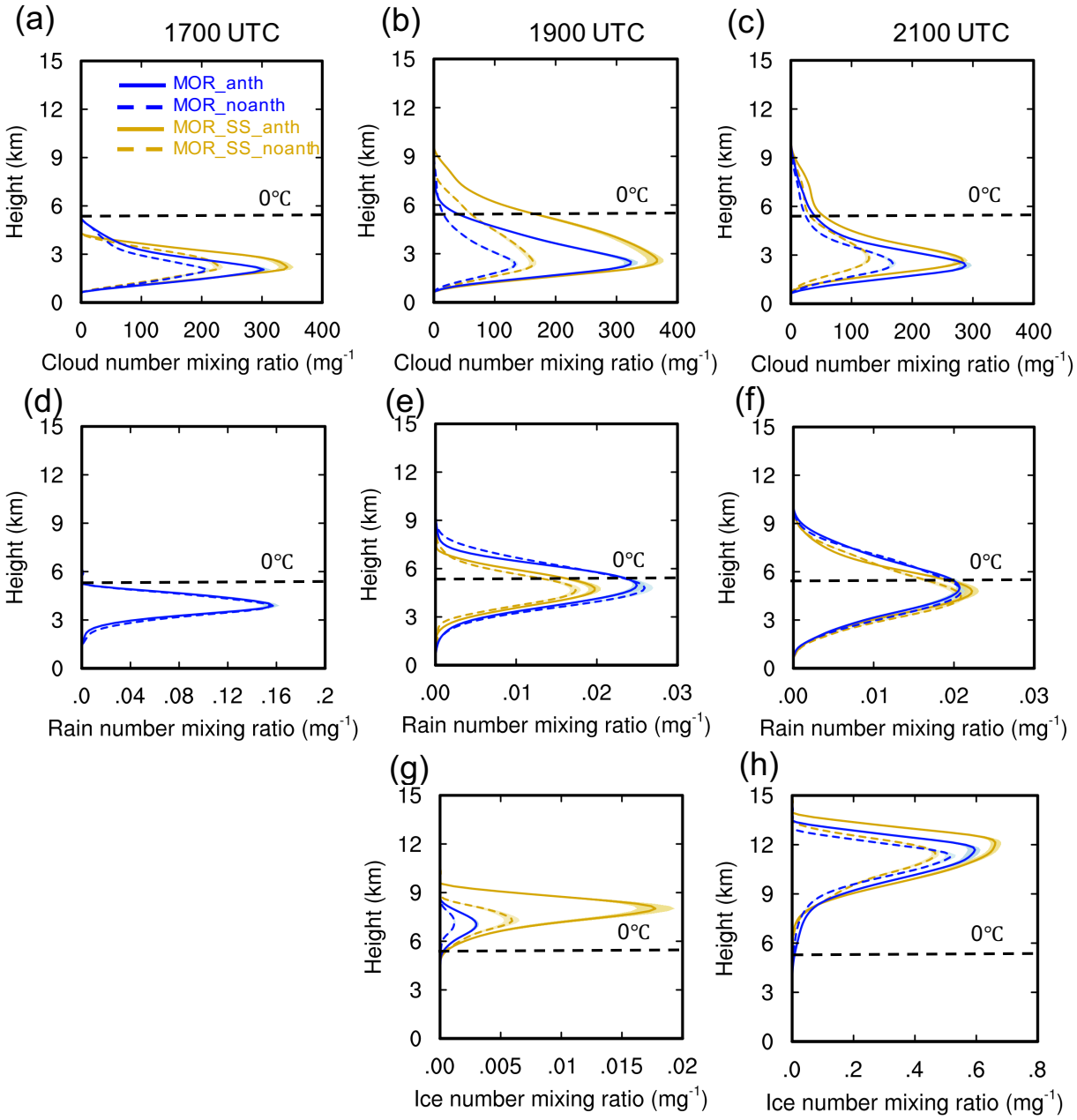

868

869 **Figure 18** Same as Figure 17, but for hydrometeor number mixing ratio.

870